Supplementary Information

Small molecule inhibition of Wnt signaling through activation of Casein Kinase 1 alpha

Curtis A. Thorne[1], Alison J. Hanson[1], Judsen Schneider[1], Emilios Tahinci[1], Darren Orton[3,8], Christopher S. Cselenyi[1], Kristin K. Jernigan[1], Kelly C. Meyers[1], Brian I. Hang[1], Alex G. Waterson[3], Kwangho Kim[3], Bruce Melancon[3], Victor P. Ghidu[3,7], Gary A. Sulikowski[3], Bonnie LaFleur[4,6], Adrian Salic[5], Laura A. Lee[1, 2], David M. Miller, III[1], and Ethan Lee[1, 2,3,9]

1. *Department of Cell and Developmental Biology, Vanderbilt University Medical Center, Nashville, TN, 37232-8240, USA*

2. Vanderbilt Ingram Cancer Center, Vanderbilt University School of Medicine, Nashville, Tennessee 37232

3. Vanderbilt Institute of Chemical Biology, Vanderbilt University, Nashville, TN 37232

4. Department of Biostatistics, Vanderbilt University, Nashville, TN 37232

5. Department of Cell Biology, Harvard Medical School, 250 Longwood Ave., Boston, MA 02115

6. Present address: Division of Epidemiology and Biostatistics, Mel and Enid Zuckerman College of Public Health, Tucson, AZ, 85724

7. Present address: Moulder Center for Drug Discovery Research, Temple University School of Pharmacy, Philadelphia, PA 19140

8. StemSynergy Therapeutics Inc., 4300 E. Tradewinds Avenue, Lauderdale by the Sea, FL 33308

Correspondence to: Ethan Lee[9] Correspondence and request for materials should be addressed to E.L. (E-mail: ethan.lee@vanderbilt.edu)

Supplementary Results

Supplementary Figure 1. A model of the effects of pyrvinium on multiple levels of the Wnt pathway. Inhibition of Wnt signaling by pyrvinium is due to allosteric activation of CK1α to regulate the stability of β-catenin and Axin in the cytoplasm and Pygopus and TCF/Lef1 in the nucleus.

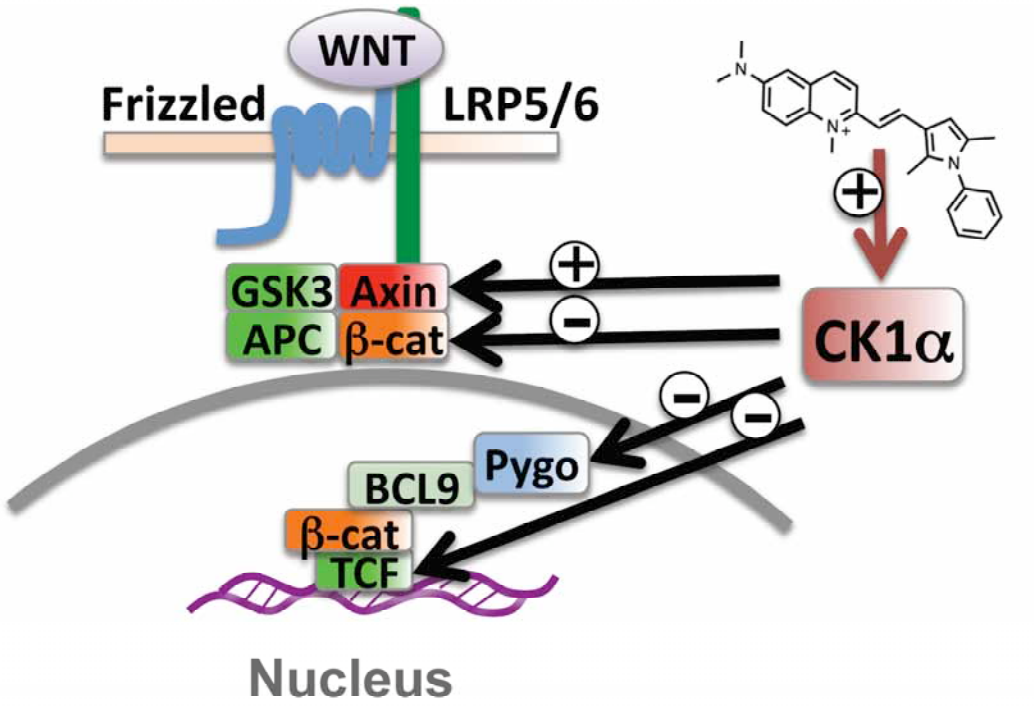

Supplementary Figure 2. Establishment of a *Xenopus* egg extract screen to identify modulators of the Wnt pathway. (**a**) Schematic of high-throughput screen assay. β-catenin-firefly luciferase (β-catenin-FLuc), Axin-*Renilla* luciferase (Axin-RLuc), and LRP6ICD were added to *Xenopus* egg extract and aliquoted into 384-well plates at 4°C. Compounds from chemical libraries were added and plates incubated at 25°C for 4 hours. β-catenin-FLuc and Axin-RLuc activities were measured by dual luciferase assay. "H" and "L" represent high and low luciferase signals, respectively. **(b)** β-catenin-FLuc and Axin-RLuc are regulated by LRP6ICD in a concentration-dependent manner in *Xenopus* egg extract. Extract was prepared as described in methods. The mean ± s. e. m. of the signal remaining after 4 hours is shown (performed in duplicate, graphed as percentage of total åresponse). (**c**) Scatter plot of change in standard deviation (ΔSD) of normalized β-catenin/Axin ratios for FDA-approved compounds from NINDS library. Unshaded regions represent compounds with activities greater than 3 standard deviations (SD) from the mean. Pyrvinium pamoate is circled in red.

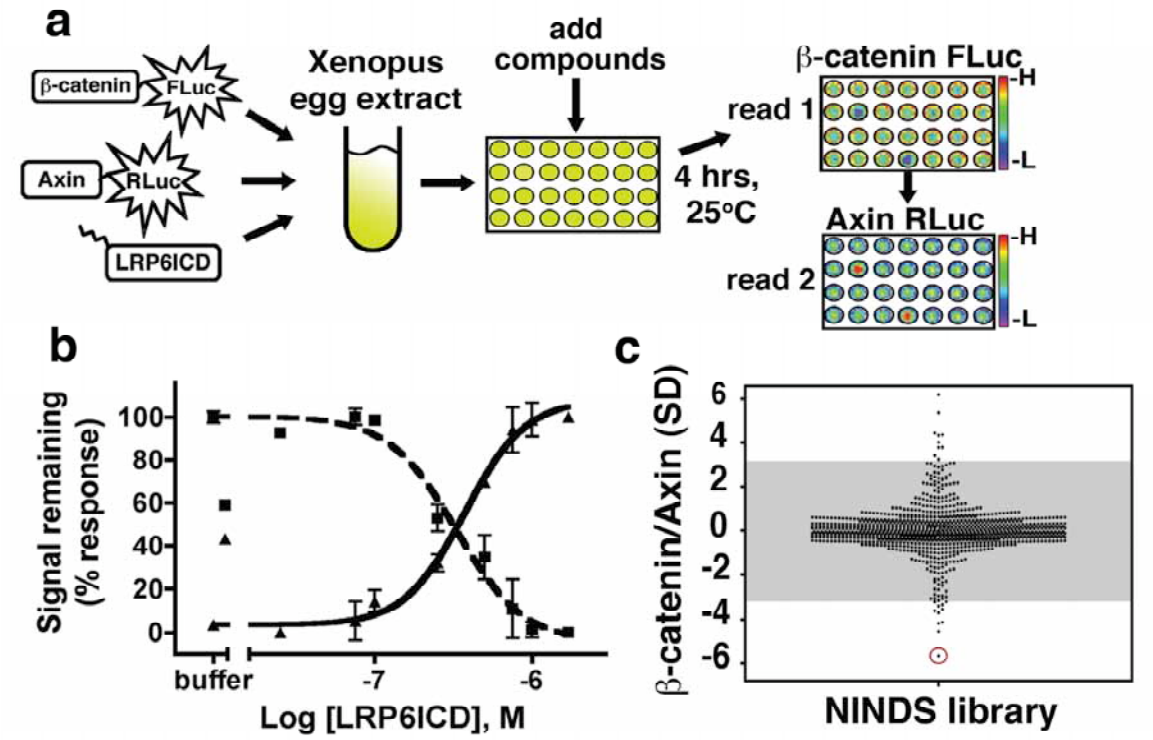

Supplementary Figure 3. Pyrvinium promotes and inhibits β-catenin and Axin degradation, respectively, in *Xenopus* extract. (a, b) Pyrvinium reverses the effects of LRP6ICD on β-catenin and Axin stability in *Xenopus* extracts. β–Catenin-FLuc **(a)** or Axin-RLuc **(b)** were added to extract in the presence of buffer, LRP6ICD, or LRP6ICD + 100 μM pyrvinium pamoate. Aliquots were removed at the indicated times and luciferase assays performed in triplicate in two independent experiments. Mean ± s.e.m. is shown. **(c,d)** Radiolabeled β-catenin or Axin was added to *Xenopus* extract minus or plus pyrvinium (100 μM) as shown in the presence (**c**) or absence (**d**) of LRP6ICD (200 nM). Samples were removed at indicated times and processed for SDS-PAGE/autoradiography. (**e**) LRP6 inhibition of GSK3-mediated β-catenin phosphorylation is reversed by pyrvinium. *Xenopus* extracts treated with LRP6ICD (200 nM) and pyrvinium as indicated were immunoblotted for total β-catenin or phospho-β-catenin (GSK3 sites required for degradation). Uncropped images of immunoblots are shown in **Supplementary Figure 19.**

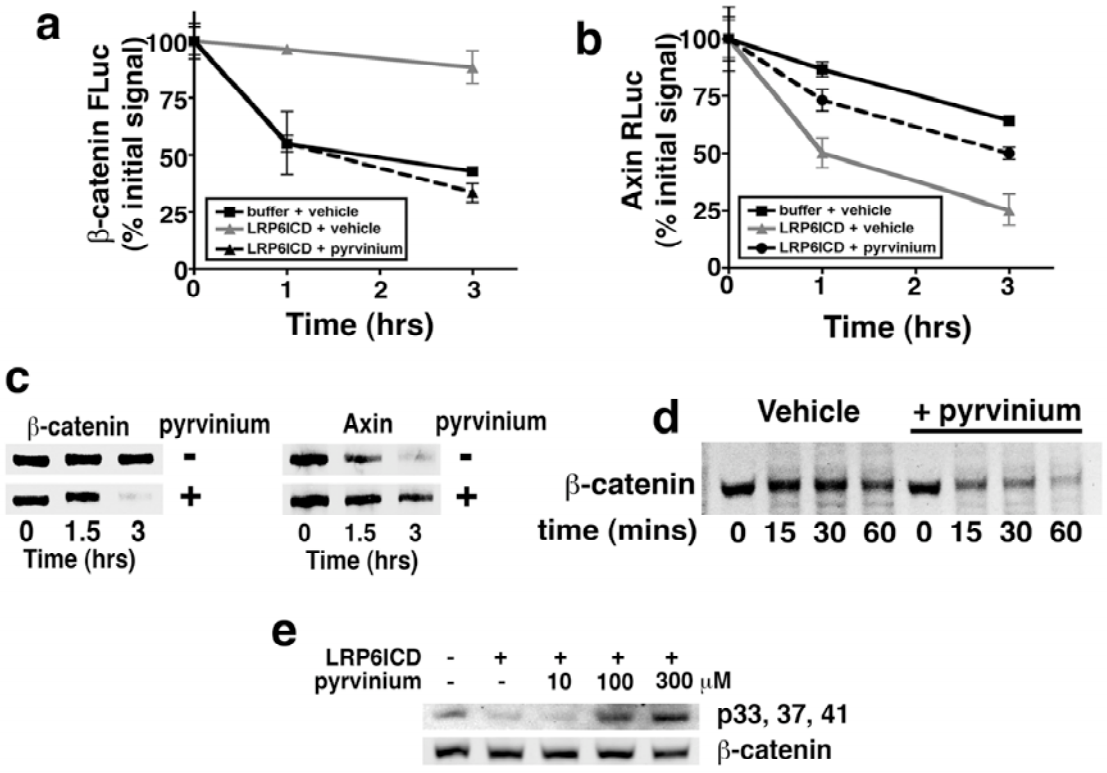

Supplementary Figure 4. Pyrvinium selectively inhibits Wnt signaling in cultured cells. (a, b) Pyrvinium does not affect BMP4, TGF-α, IL-4, or Notch signaling pathways. **(a)** Pyrvinium has no observable biochemical effect on BMP4, TGF-α, or IL-4 signaling. HEK 293 cells were pretreated with pyrvinium pamoate (100 nM) for 2 hours prior to addition of ligands (BMP4, 50 ng/ml; TGF-α, 10 nM; or IL-4, 0.1 ng/ml) and lysed 30 minutes later for immunoblotting using antibodies against downstream effectors (pSMAD1/5, pMAPK, or pSTAT6 respectively). **(b)** Pyrvinium pamoate does not block BMP4, TGF-α, IL-4, or Notch pathway reporter gene activation. BMP4, TGF-α, and IL-4 treated cells were transfected with luciferase-based reporter constructs as described in methods and treated as indicated for 24 hours. For activation of the Notch pathway, NotchICV was cotransfected with a luciferase-based reporter construct as previously described[1]. Mean ± s.e.m. of luciferase signal normalized to a cotransfected Renilla luciferase control is shown (performed in quadruplicate). (**c-g**) Regulation of Wnt signaling by pyrvinium salts and a pyrvinium analog. Structures of **(c)** pyrantel pamoate (**2**) and (**d**) pyrvinium iodide (**3**). (**e**) Both the iodide and pamoate salts of pyrvinium inhibited TOPflash activation with essentially identical EC_{50}s (~10 nM). (**f**) Structure of VU-WS211 (**4**), a pyrvinium analog. (**g**) VU-WS211 fails to inhibit TOPflash. HEK 293 STF cells were treated with Wnt3a and compounds. For graphs **b**, **e**, and **g**, mean ± s.e.m. of TOPflash activity normalized to cell number are shown (performed in triplicates). Uncropped images of immunoblots are shown in **Supplementary Figure 20.**

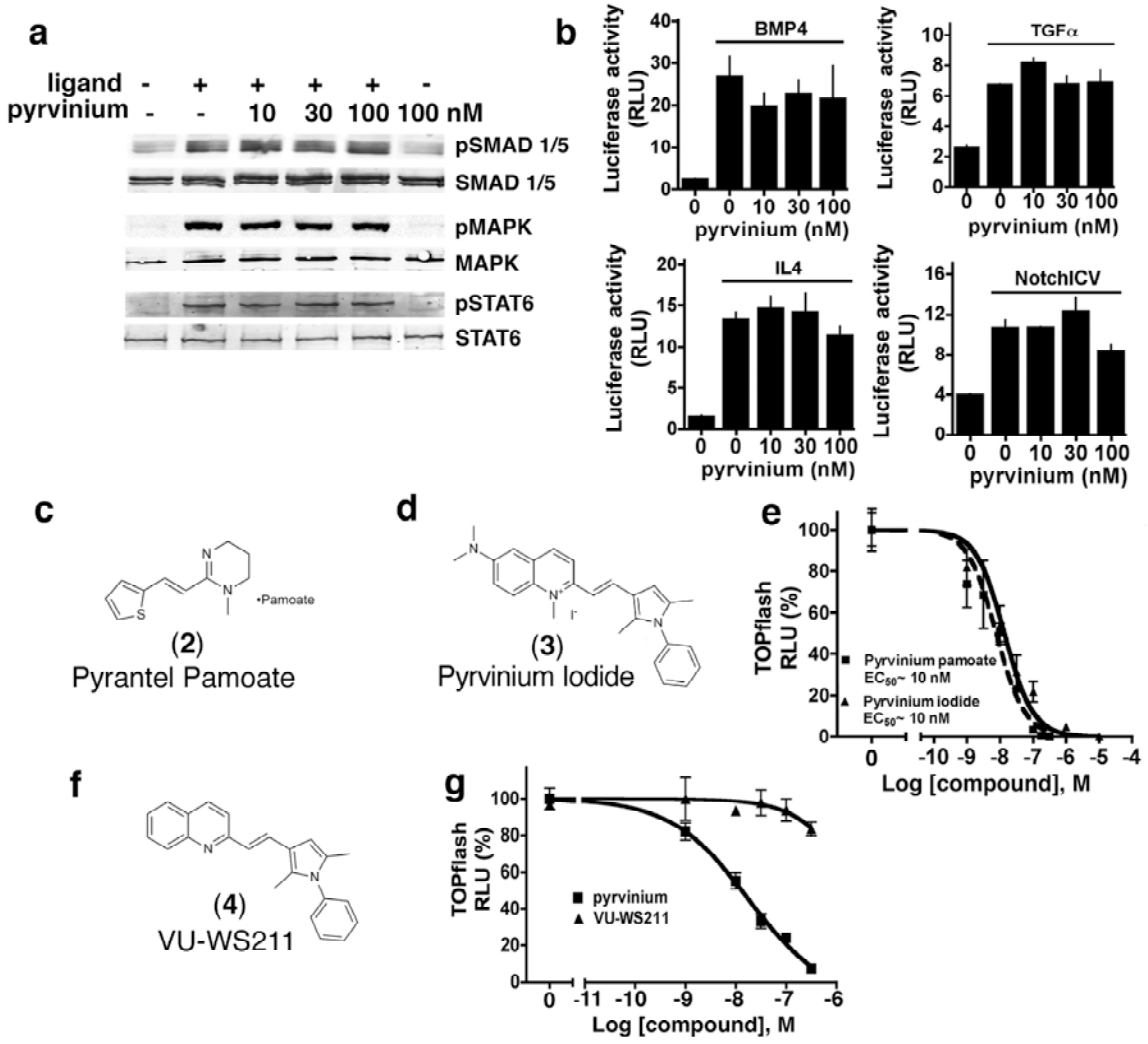

Supplementary Figure 5. Pyrvinium inhibits Wnt signaling in multiple model systems. (a,b) Comparison of the effects of pyrvinium and VU-WS211, a structurally related inactive analog on axis formation in *Xenopus*. (**a**) VU-WS211 fails to inhibit Xwnt8-induced secondary axis formation in *Xenopus*. Embryos (4-8 cell stage) were injected ventrally with *Xwnt8* mRNA (0.5 pg) plus vehicle, pyrvinium pamoate, or VU-WS211 (100 μM each) and scored for axis duplication. (**b**) Dorsal injection of pyrvinium ventralizes *Xenopus* embryos in a dose-dependent manner. Embryos were injected dorsally with vehicle, pyrvinium pamoate, or VU-WS211 and scored for ventralization. Dorsal anterior index (DAI) of ventralized embryos ranged from 2-4. n=number of embryos injected. (**c**) Pyrvinium does not inhibit expression of *XMyf5* and *Xbra* (Xnr-2 and bFGF target genes) in *Xenopus* animal cap explants. Embryos (2-cell stage) were injected with *Xnr-2* mRNA (100 pg) plus pyrvinium pamoate (100 μM) or vehicle (top panel). Animal caps were excised, total RNA extracted, and RT-PCR performed. Animal caps were treated with bFGF (50 ng/ml) for 2 hours prior to extraction of total RNA (bottom panel). WE, whole embryo. RT, reverse transcriptase. Ornithine decarboxylase (ODC), loading control. (**d**,**e**) Pyrvinium inhibits Wg signaling in *Drosophila* S2 cells. (**d**) Cells stably transfected with a TOPflash reporter were treated with Wg plus VU-WS211 or pyrvinium pamoate. Graph represents mean ± s.e.m. of luciferase signal normalized by cell number (performed in quadruplicate). (**e**) Pyrvinium pamoate decreases cellular Armadillo levels. Lysates from S2 cells treated with Wg minus or plus pyrvinium (100 nM) were immunoblotted for Armadillo. Tubulin, loading control. (**f-i**) Pyrvinium induces defects in *C. elegans* development that phenocopy Wnt inhibition. (**f**) Pyrvinium enhances Q cell migration defect of hypomorphic TCF (*pop-1*) mutants. *pop-1*; *mec-7*::GFP worms were treated with pyrvinium pamoate and QL cell migration scored. n=number of embryos. p<0.05 for vehicle vs. 100 μM pyrvinium. (**g**) Vulval morphology (arrowheads) is defective in pyrvinium pamoate-treated animals. (**h,i**) Quantification of vulval morphology (p<0.001 for the pyrvinium vs. vehicle or VU-WS211) (**h)** or egg retention (p<0.0005) (**i**) in *C. elegans* treated with pyrvinium pamoate or VU-WS211. Scale bar, 1 μm. n=number of animals. Vehicle is 0.1% ethanol. Uncropped images of immunoblots and agarose gels are shown in **Supplementary Figure 20.**

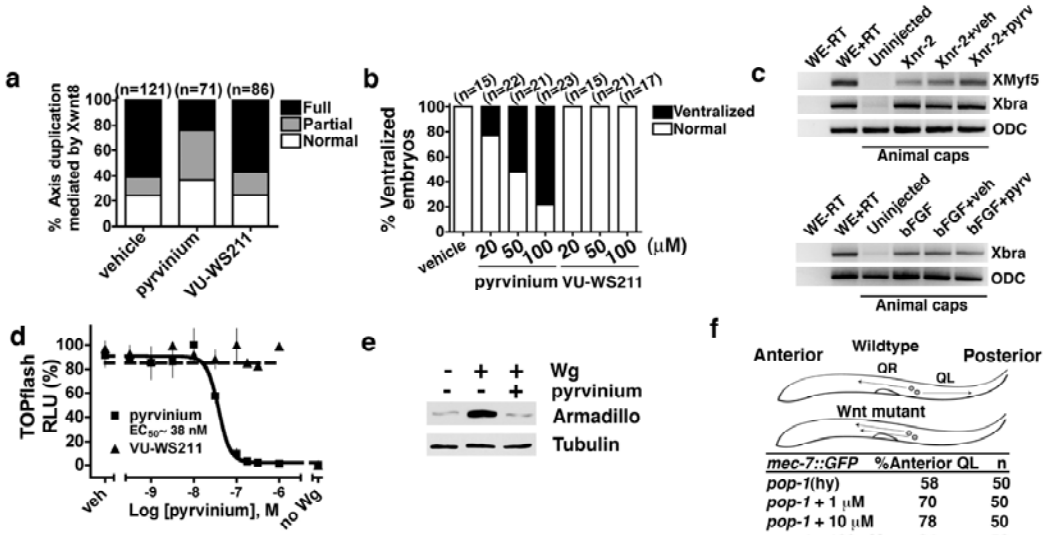

mec-7::GFP	%Anterior QL	n
pop-1(hy)	58	50
pop-1 + 1 μM	70	50
pop-1 + 10 μM	78	50
pop-1 + 100 μM	84	50

h Vulval Morphology

Treatment	Normal	n
Vehicle	100%	30
pyrvinium (10 μM)	67%	30
VU-WS211 (10 μM)	100%	150

i Egg Retention in Uterus

Treatment	Avg#Eggs	n
Vehicle	9.9 ± 3.9	65
pyrvinium (10 μM)	12.9 ± 4.3	65

Supplementary Figure 6. Pyrvinium binds and activates CK1α *in vitro*. (**a**) Fluorescence signal of pyrvinium. The indicated concentrations of pyrvinium pamoate were excited at 540λ and emission signals determined at 590λ. (**b**) Pyrvinium binds CK1 *in vitro*. β-catenin, Axin, GSK3, and CK1δ1-317 (0.5 μg each) were spotted on nitrocellulose, incubated with pyrvinium pamoate (10 nM), and fluorescence detected (**c**,**d**). Pyrvinium stimulates phosphorylation of β-catenin by CK1 *in vitro*. (**c**) Purified β-catenin and CK1 (100 nM each) were incubated in a kinase reaction containing [γ^{32}P]ATP in the absence or presence of pyrvinium pamote (1 nM). Samples were analyzed by SDS-PAGE/autoradiography. (**d**) CK1 and β-catenin (100 nM each) were incubated in a kinase reaction and phospho-Ser45 β-catenin (p45) detected by immunoblotting. (**e**) Pyrvinium stimulates *in vitro* phosphorylation of Axin by CK1 in a dose-dependent manner. Purified Axin and CK1 (100 nM each) were incubated in a kinase reaction containing [γ^{32}P]ATP in the absence or presence of varying concentrations of pyrvinium pamoate. Samples were analyzed by SDS-PAGE/autoradiography. Recombinant CK1δ1-317 was used as the source of CK1. (**f**) Diagram of CK1 isoforms. Autophosphorylation of the C-terminal extensions of CK1 isoforms has been shown to inhibit kinase activity. Of particular note is that CK1α contains a shorter C-terminal extension compared to the other CK1 isoforms. CK1δ1-317 is a truncated form that lacks a portion of the C-terminal extension of CK1δ. Asterisks mark isoforms activated by pyrvinium (α and δ1-317). (**g**) Pyrvinium affects the conformation of CK1α *in vitro* as assayed by limited trypsin proteolysis. Sliver stained gel indicate prominent CK1α fragments (arrowheads) that only appear when purified, recombinant CK1α is trypsinized in the presence of pyrvinium pamoate (100 nM). No observable difference in the digest pattern is detected when GSK3 is trypsinized in the absence or presence of pyrvinium pamoate. Uncropped images of immunoblots are shown in **Supplementary Figure 21.**

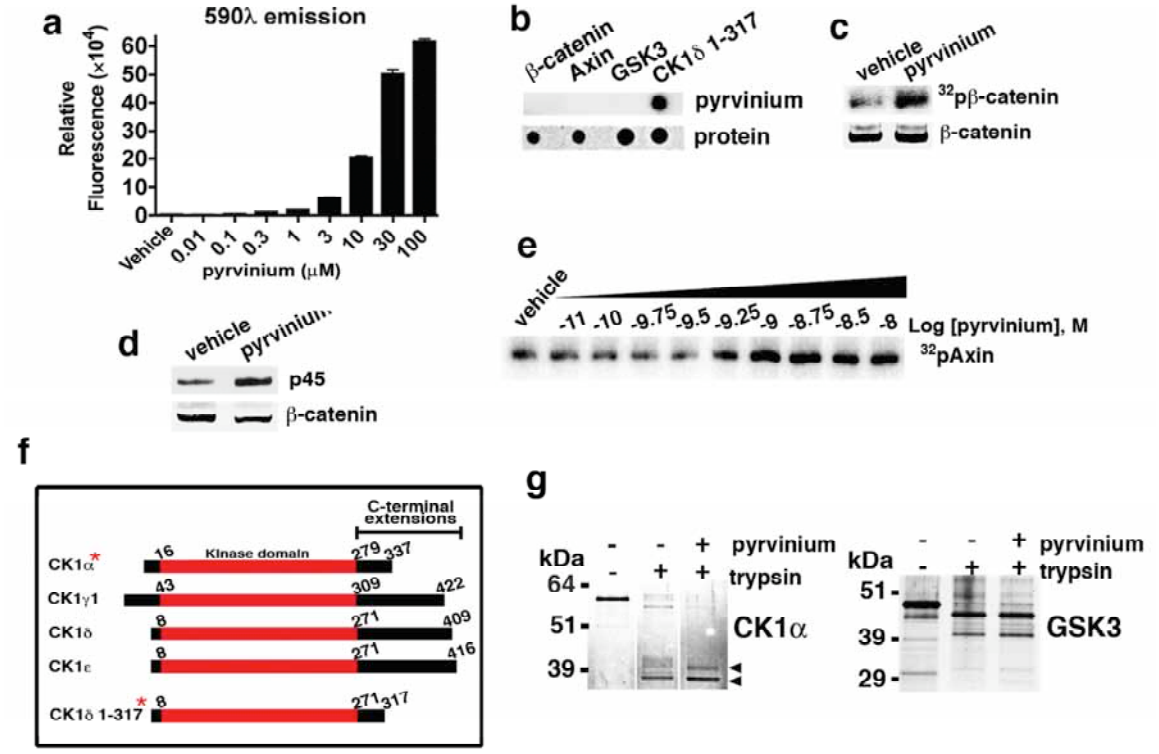

Supplementary Figure 7. Activation of intracellular CK1α by small molecules inhibits Wnt signaling. (**a**) Pyrvinium activates CK1α in cultured cells. HEK 293 cells overexpressing CK1α were treated with pyrvinium pamoate (100 nM). CK1α immunoprecipitated from lysates was incubated with purified β-catenin (100 nM) in a kinase assay containing [γ^{32}P]ATP. Samples were processed for SDS-PAGE/autoradiography. As control, immunoprecipitates were treated with the CK1 inhibitor, CKI-7 (1 μM). Immunoblots of β-catenin and CK1α show equivalent amounts of protein were used in each sample. (**b**) Pyrvinium co-immunoprecipitates with CK1α. HEK 293 cells expressing HA-GSK3, HA-CK1α, or HA alone (vector control) were treated with pyrvinium pamoate (100 nM). HA immunoprecipitates were analyzed by LC-MS. Graph represents mean ± s.e.m. of relative abundance of pyrvinium normalized to bead control (performed in triplicate). Immunoblots show that comparable amounts of HA-tagged proteins and light chain IgG (LC-IgG) were present in the immunoprecipitates. (**c-g**) Derivatives of pyrvinium that inhibit Wnt signaling also activate CK1α. (**c**) Structure of VU-WS113 (**5**). (**d,e**) HEK 293 STF cells were treated with Wnt3a and the indicated concentrations of VU-WS113 **(d)** or VU-WS211 **(e)** and assayed for luciferase activity. Mean ± s.e.m. of TOPflash activity normalized to cell number is shown (performed in quadruplicate and displayed as percent response). (**f**) CK1α (100 nM) was incubated with recombinant casein (100 nM) in the presence or absence of compounds in a kinase reaction containing [γ^{32}P]ATP. Samples were analyzed by SDS-PAGE/autoradiography and the extent of ^{32}P incorporation into casein (in the presence of pyrvinium relative to vehicle) assessed. Mean ± s.e.m. is shown (performed in triplicates). Uncropped images of immunoblots are shown in **Supplementary Figure 22.**

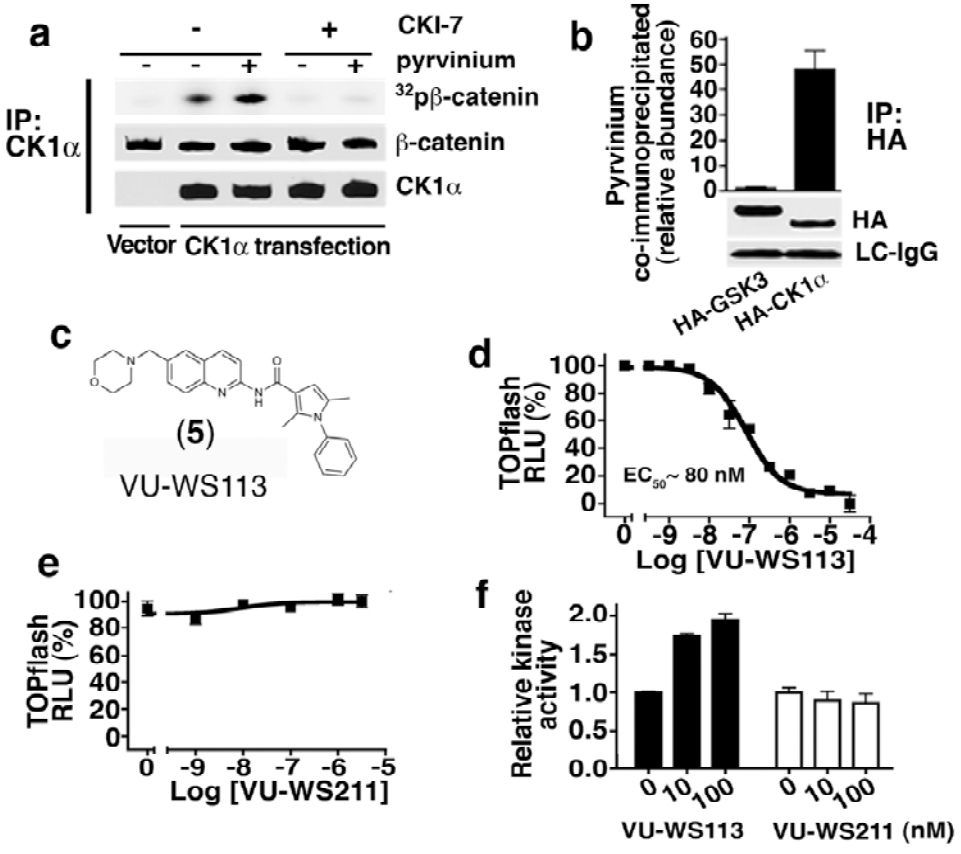

Supplementary Figure 8. Pyrvinium inhibits Wnt signaling downstream of stabilized β-catenin. (**a**) Pyrvinium inhibits Wnt signaling in colon cancer cells. Cells transfected with TOPflash reporter and *Renilla* luciferase control plasmid were treated with pyrvinium pamoate. Lysates were assayed for luciferase activity. Graph shows mean ± s.e.m. of luciferase signal normalized by cell number (performed in quadruplicate). (**b-f**) Inhibition of Wnt signaling by an Axin stabilizing compound, IWR-1 (**6**), differs from that of pyrvinium. (**b**) Structure of IWR-1. (**c,d**) HEK 293 STF reporter cells were treated with Wnt3a (**c**) or LiCl (50 mM) (**d**) with indicated doses of IWR-1. (**e,f**) Compared to the inhibitory effects of pyrvinium pamoate on TOPflash activity, IWR-1 is less potent in SW480 cells (**e**) and is ineffective in HCT116 WTKO cells (**f**). Graphs show mean ± s.e.m. of luciferase signal normalized by cell number (performed in quadruplicate). (**g,h**) Pyrvinium has no effect on β-catenin nuclear accumulation in cells treated with lithium. (**g**) HEK 293 cells were treated with LiCl (50 mM) and/or pyrvinium pamoate. Cytoplasmic and nuclear fractions were immunoblotted for β-catenin. Purity of nuclear and cytoplasmic preparations was assessed by immunoblotting for acetylated Histone H3 and actin, respectively. NaCl and vehicle were used in LiCl and pyrvinium minus lanes, respectively. (**h**) IEC-6 cells were treated with LiCl (50 mM) and/or pyrvinium pamoate (100 nM), fixed, and stained for β-catenin and DNA. Scale bar, 10 μm. Uncropped images of immunoblots are shown in **Supplementary Figure 23.**

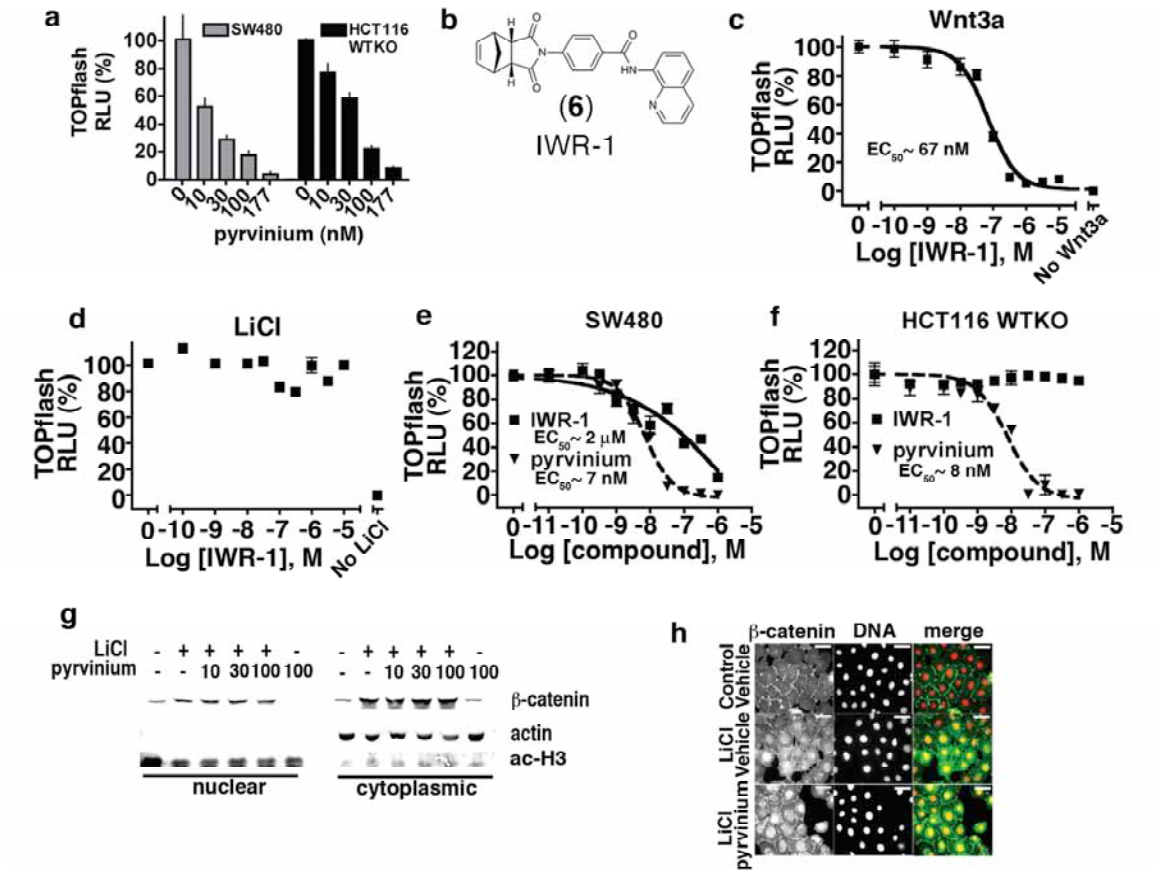

Supplementary Figure 9. Pyrvinium decreases β-catenin and increases Axin levels in a colon cancer line mutant for APC. SW480 cells were treated with pyrvinium pamoate (100 nM) and lysates immunoblotted for β-catenin and Axin. Tubulin, loading control. Uncropped images of immunoblots are shown in **Supplementary Figure 23.**

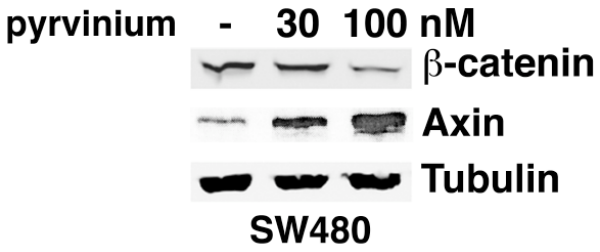

Supplementary Figure 10. Pyrvinium promotes degradation and CK1α phosphorylation of Pygopus. (**a**) Effects of pyrvinium on levels of overexpressed Pygopus and β-catenin in HCT116 WTKO and SW480 cell lines. Transfected cells expressing HA-tagged Pygopus were treated with pyrvinium pamoate (100 nM). Lysates were immunoblotted for HA and β-catenin. β-galactosidase (β-gal), loading control. (**b**) Pyrvinium reduces nuclear Pygopus levels. HeLa cells expressing GFP-Pygopus and histone H2B-mCherry (marks DNA) were treated with pyrvinium pamoate (100 nM). Scale bar, 5 μm. (**c**) Pyrvinium stimulates turnover of Pygopus in colorectal cancer lines. Extracts of HCT116 WTKO and SW480 cells treated with or without pyrvinium pamoate (100 nM) were immunoblotted for endogenous Pygopus. Tubulin, loading control. (**d**) CK1α interacts with Pygopus. HEK 293 cells expressing HA-CK1α and Myc-Pygopus were lysed for Myc immunoprecipitation. HA-CK1α and Myc-Pygopus were detected by immunoblotting with HA and Myc antibodies. WCL, whole cell lysate. (**e**) Phosphorylation of Pygopus by CK1α is enhanced by pyrvinium. HEK 293 cells expressing Myc-Pygopus were lysed for Myc immunoprecipitation, and *in vitro* kinase assays using recombinant CK1α (100 nM) were performed in the absence or presence of pyrvinium pamoate (100 nM). Uncropped images of immunoblots are shown in **Supplementary Figure 24.**

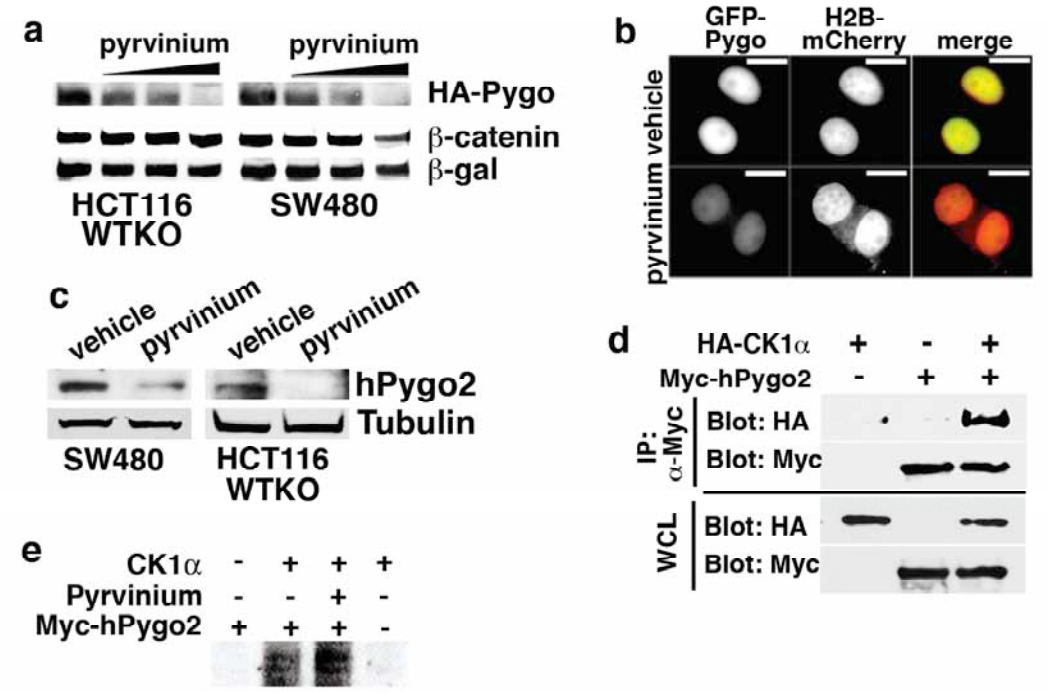

Supplementary Figure 11. Pyrvinium inhibits TCF/Lef1-mediated Wnt signaling. HEK 293 STF cells were (**a**) transfected with LEFΔN-VP16 or CMV-Luc followed by pyrvinium pamoate treatment or (**b**) transfected with LEFΔN-VP16 plus or minus HA-CK1α. Lysates were assayed for TOPflash activity and immunoblotting for HA and VP16. Tubulin, loading control. Mean ± s.e.m. of TOPflash activity is graphed (performed in quadruplicate and displayed as percent response). Uncropped images of immunoblots are shown in **Supplementary Figure 24.**

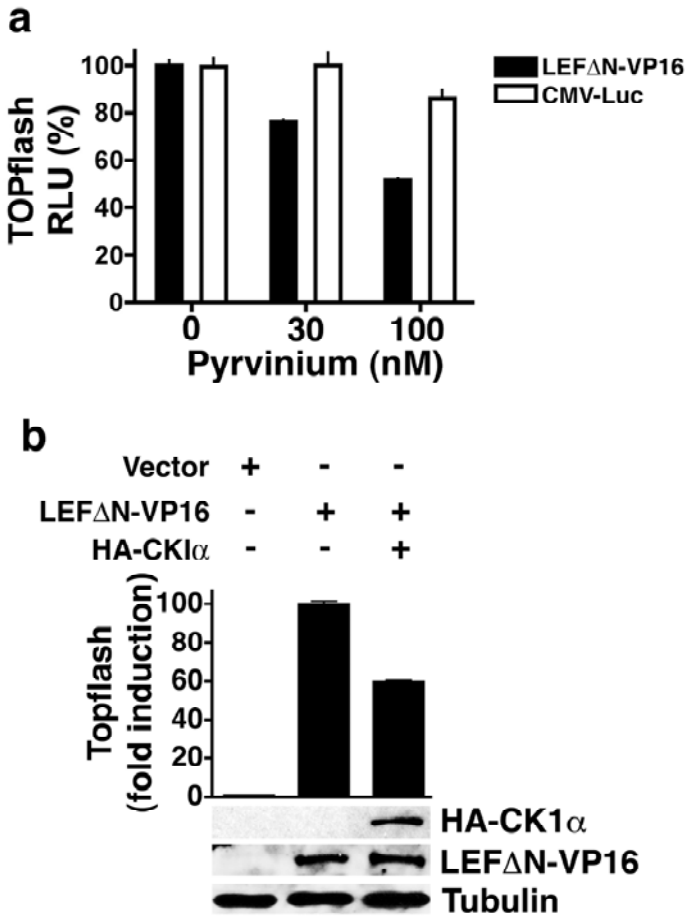

Supplementary Figure 12. Pyrvinium blocks Wnt3a-induced cellular changes and decreases levels of the nuclear proliferating marker, Ki-67. (**a**,**b**) Pyrvinium inhibits Wnt3a-induced changes in cell morphology and repression of the junction marker, ZO-1. HEK 293 cells were treated with Wnt3a in the absence or presence of pyrvinium pamoate (10 nM) for 7 days. (**a**) Phase-contrast micrographs (20X magnification) show reversion of Wnt3a-induced changes in morphology by pyrvinium pamoate. (**b**) Fluorescent micrographs (40X magnification) show that pyrvinium pamoate enhances ZO-1 staining in Wnt3a-treated cells. Phalloidin staining of actin marks the cell cortex. (**c**,**d**) Pyrvinium decreases proliferation of HCT116 WTKO cells without affecting cell-cycle phasing. (**c**) Fluorescent micrographs (100X magnification) of cells treated with or without pyrvinium pamoate (100 nM) for 48 hours, fixed, and stained for Ki-67, a proliferation marker. (**d**) Cells were treated with or without pyrvinium pamoate (100 nM) for 24 or 48 hours, fixed, stained with DAPI, and analyzed by FACS.

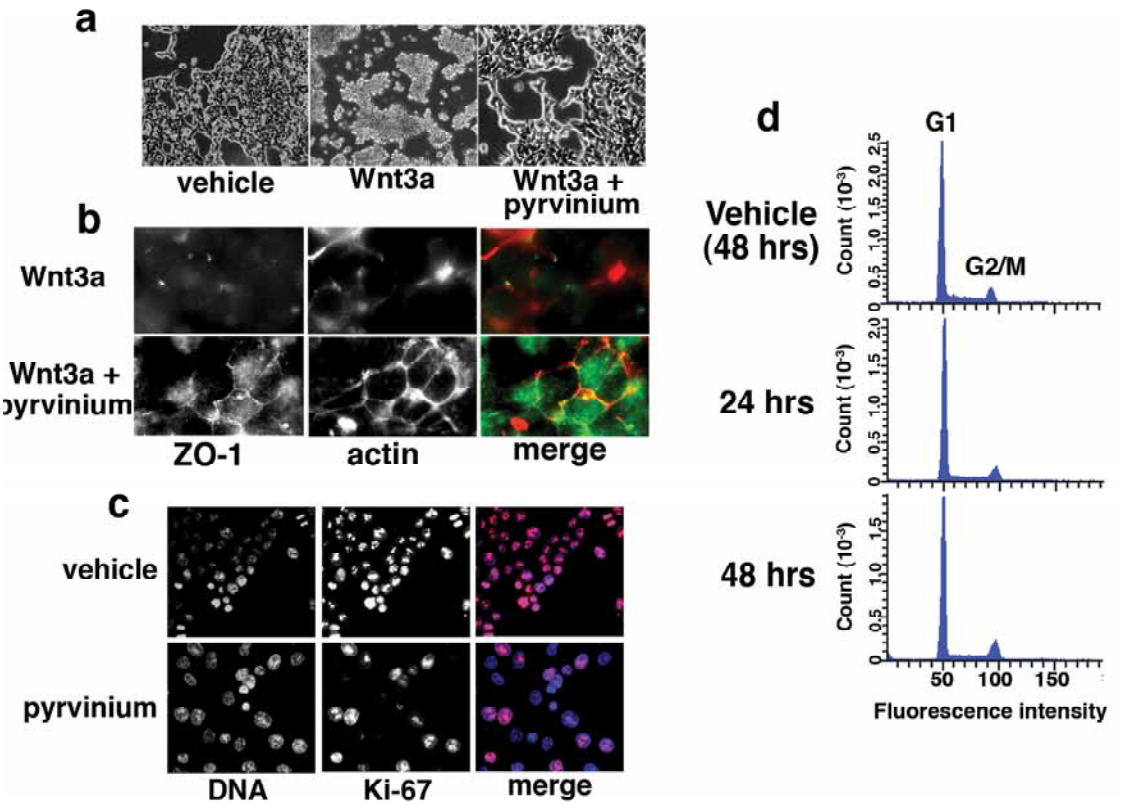

Supplementary Figure 13. Pyrvinium inhibits the growth/proliferation of cultured cancer cells in a dose-dependent manner. HCT116 cells were incubated with varying concentrations of pyrvinum pamoate and viability assessed at the indicated times using CellTiter-Fluor (Promega).

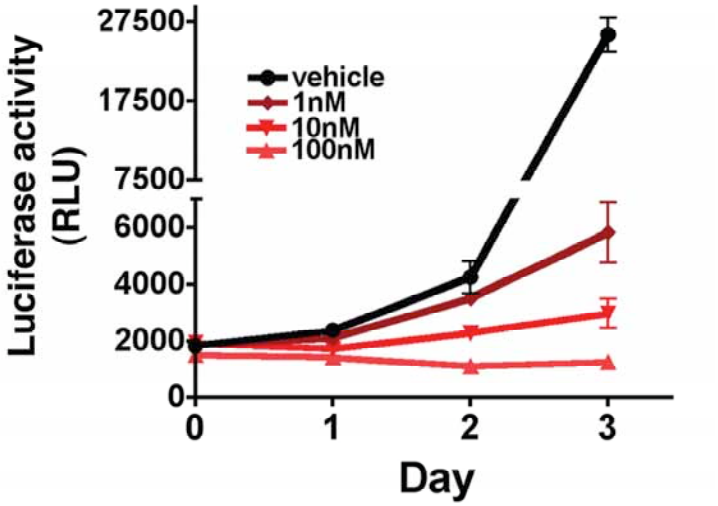

Supplementary Figure 14. Pyrvinium potentiates the apoptotic effects of 5-FU on colon cancer cells. The highly metastatic colon cancer line, SW620, was treated with combinations of pyrvinium pamoate (100 nM) and 5-FU (5 μM). (**a**) Mean ± s.e.m. of caspase 3/7 activity normalized to vehicle-treated cells is graphed (performed in triplicate). (**b**) Phase contrast micrographs (20X magnification) show enhanced blebbing (indicative of apoptosis) of cells treated with both compounds.

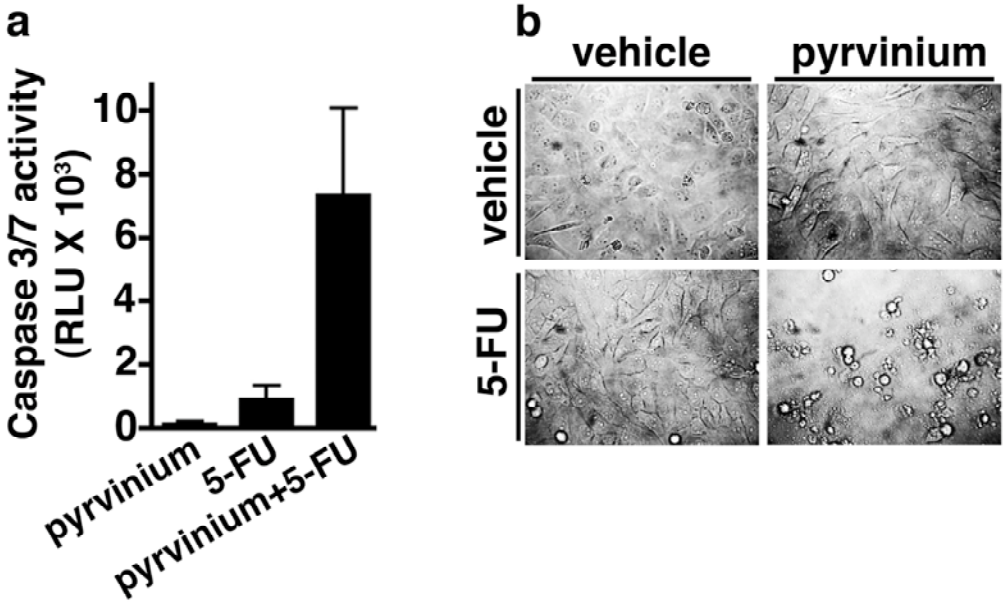

Supplementary Figure 15. Pyrvinium but not IWR-1 decreases viability of colon cancer cells under normal serum conditions. Colon cancer lines (SW480, SW620, HCT116 WTKO, and DLD-1) were treated for 72 hours with the indicated concentrations of pyrvinium pamoate or IWR-1 in normal growth media (10% FBS) and cell viability determined.

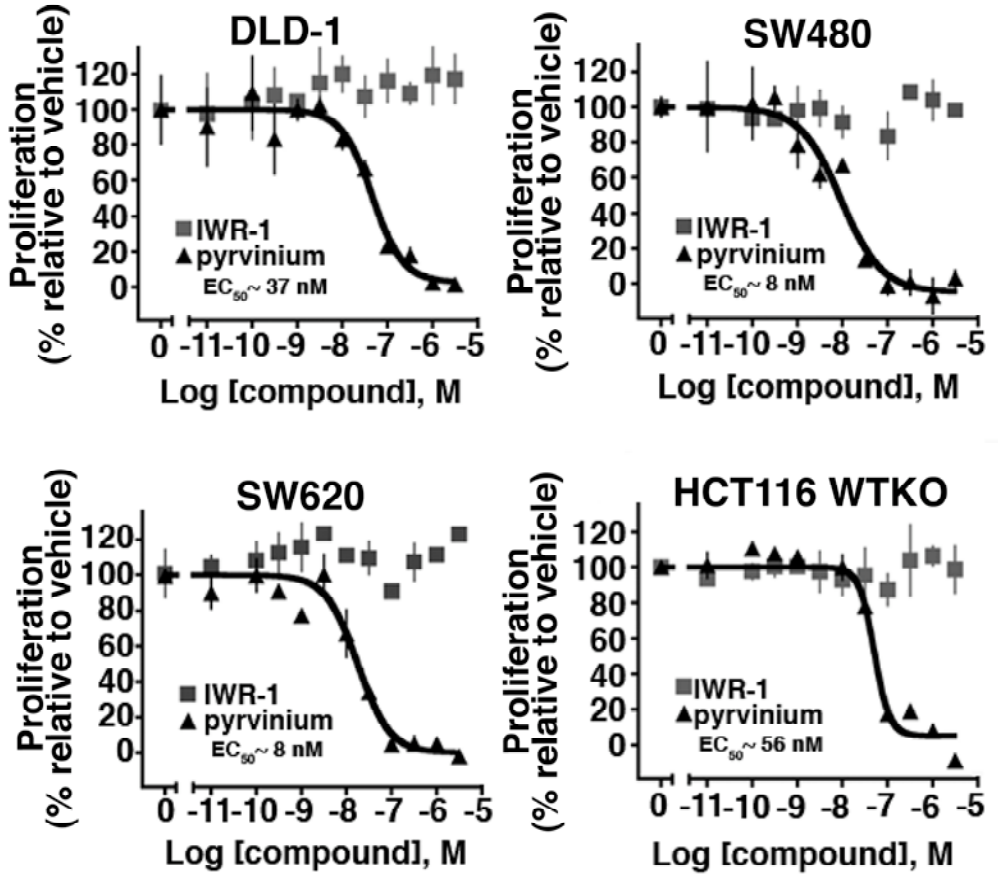

Supplementary Figure 16.

Full length gels for Figures 1 and 2.

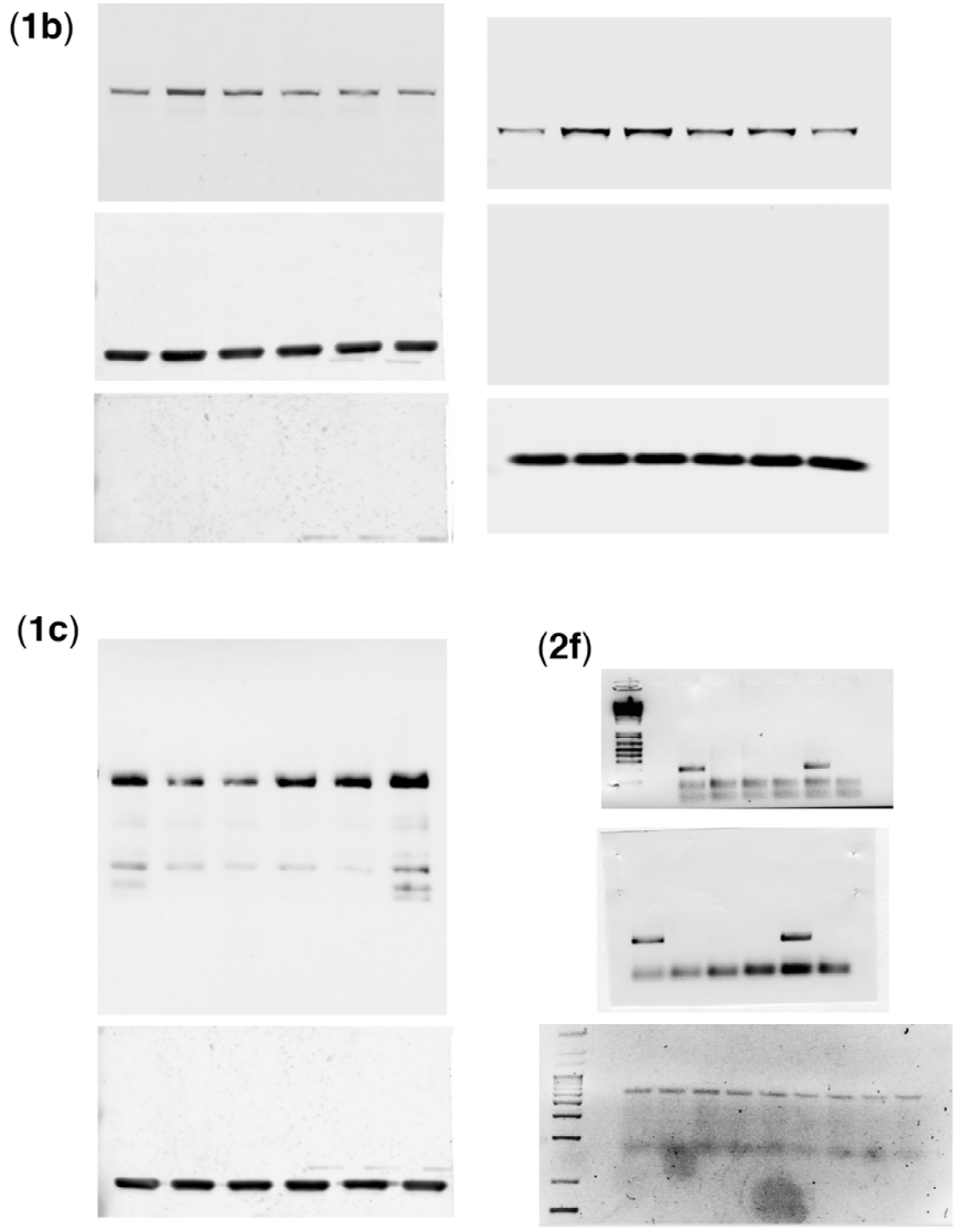

Supplementary Figure 17.

Full length gels for Figure 3.

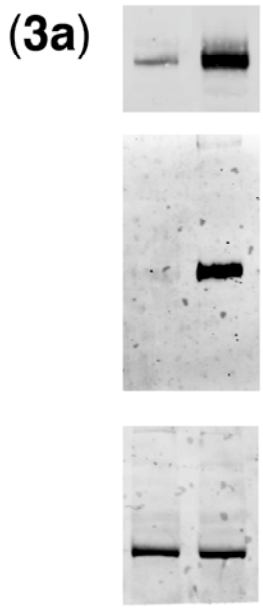

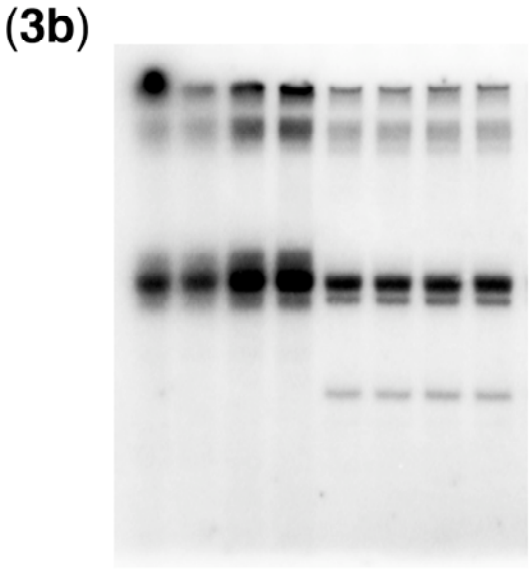

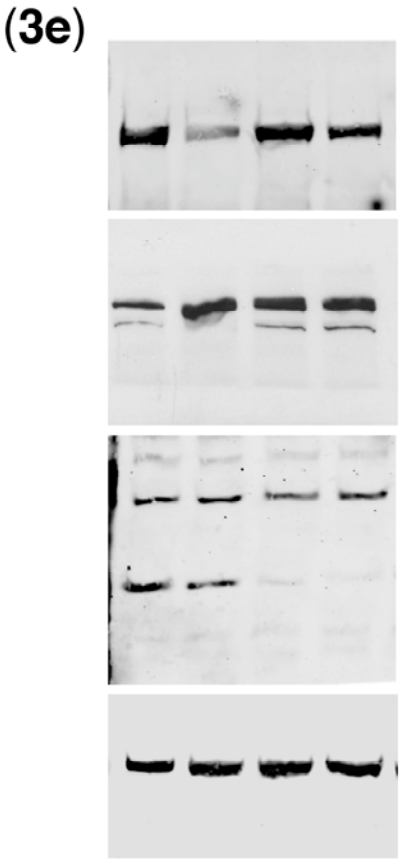

Supplementary Figure 18.

Full length gels for Figure 4.

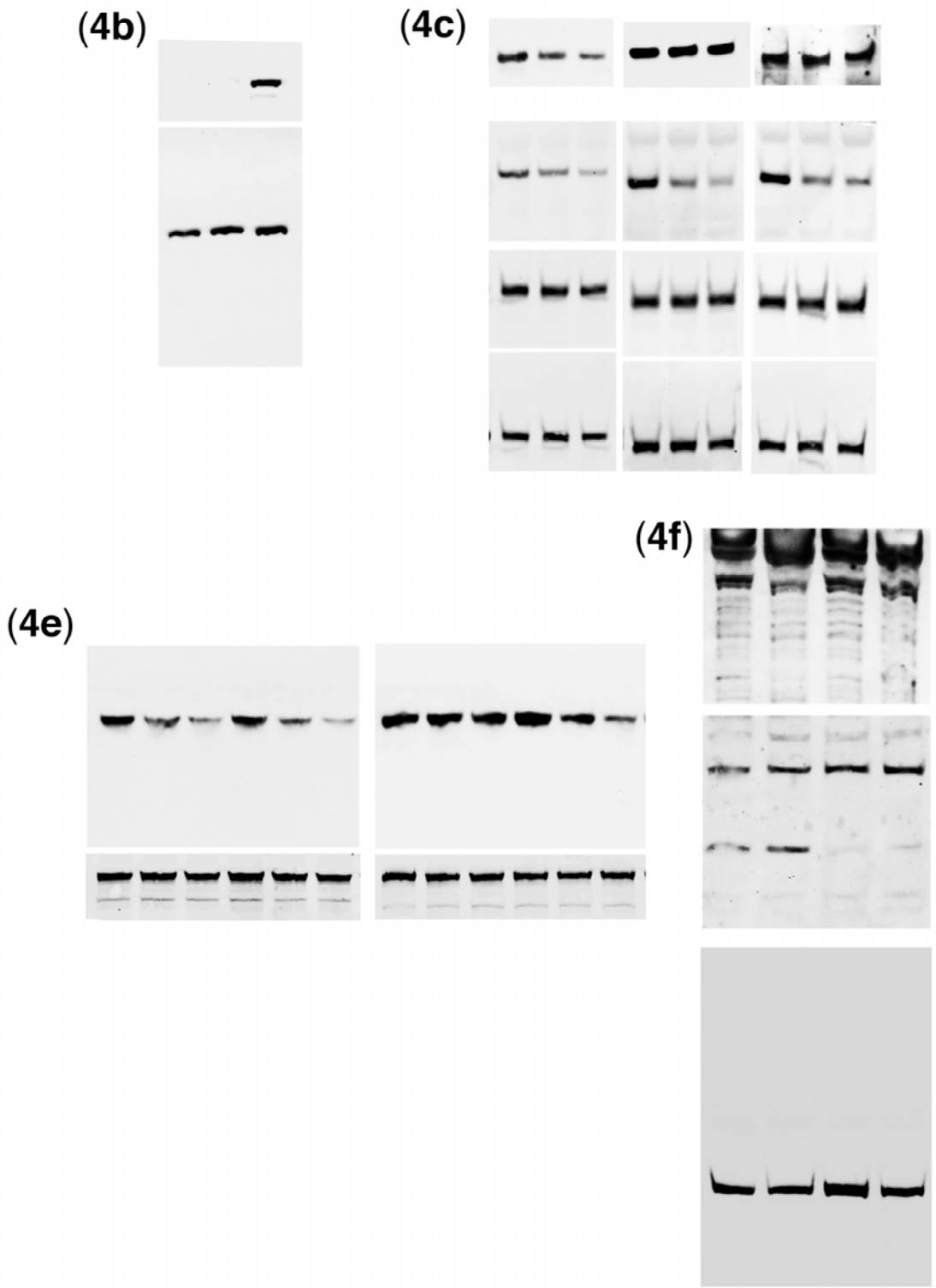

Supplementary Figure 19.

Full length gels for Supplementary Figure 3.

(Sup 3c)

(Sup 3d)

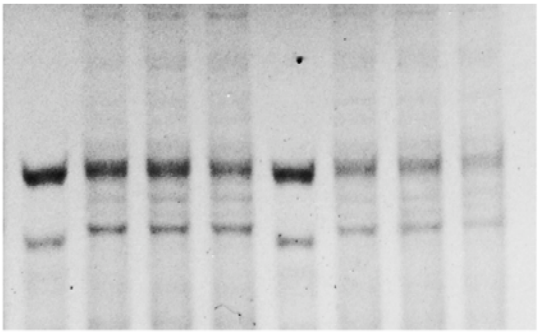

(Sup 3e)

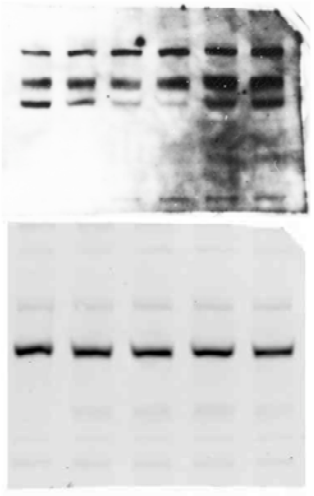

Supplementary Figure 20.

Full length gels for Supplementary Figure 4 and 5.

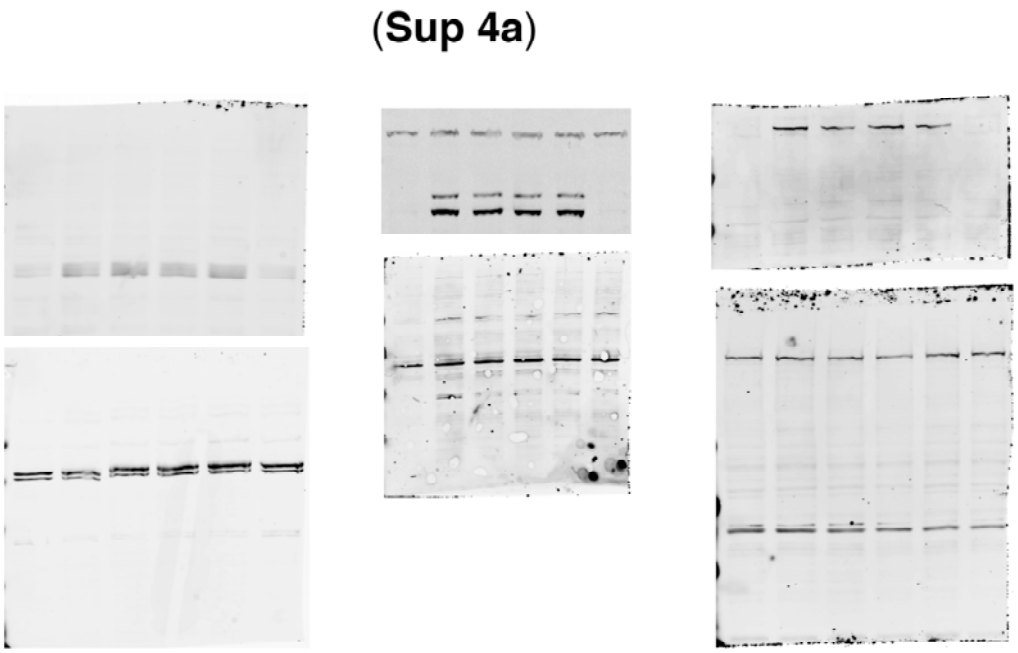

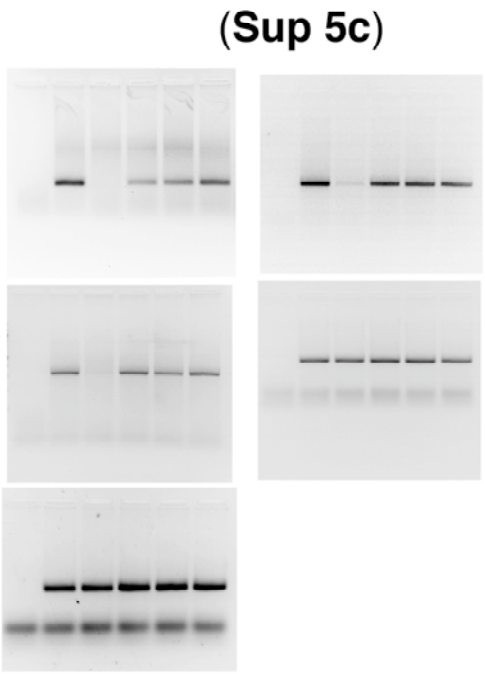

Supplementary Figure 21.

Full length gels for Supplementary Figure 6.

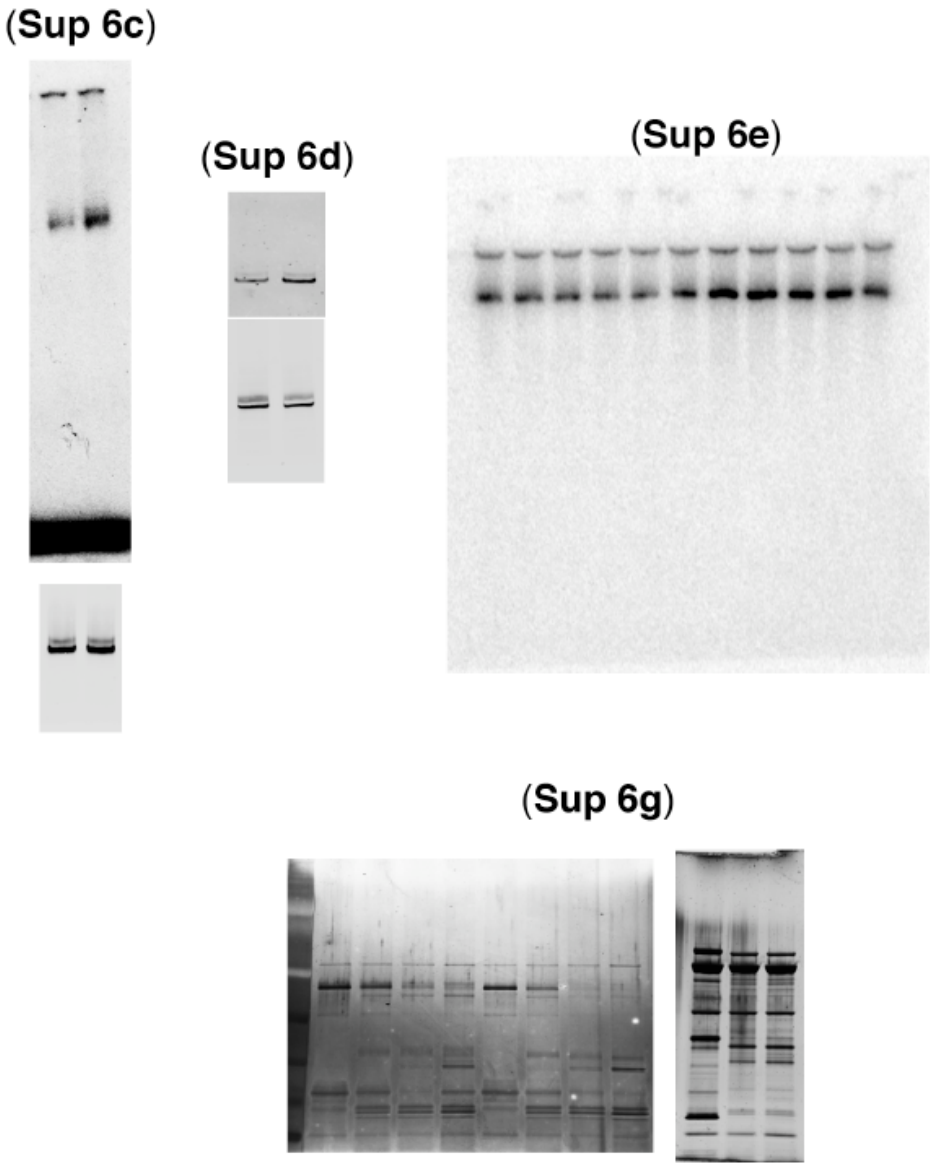

Supplementary Figure 22.

Full length gels for Supplementary Figure 7.

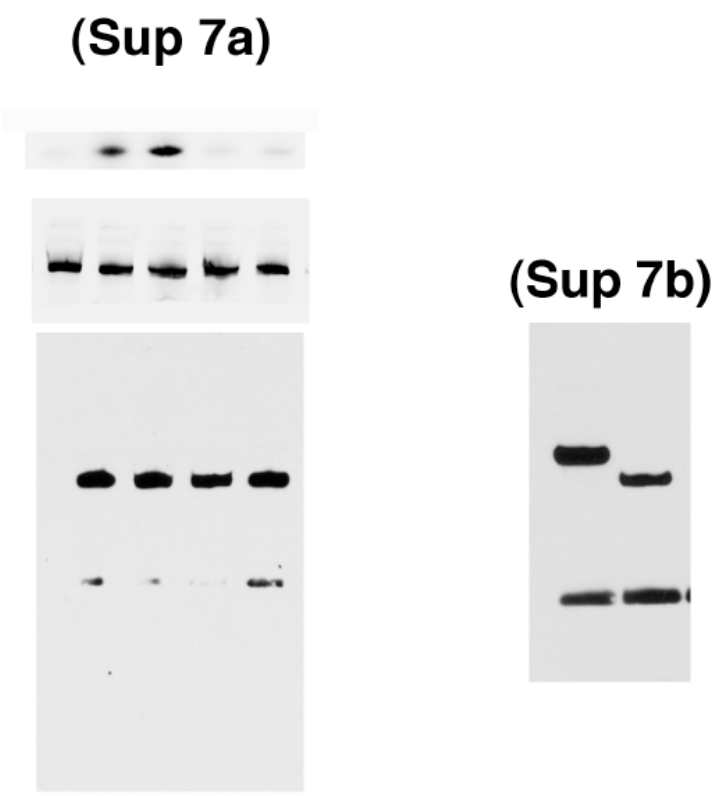

Supplementary Figure 23.

Full length gels for Supplementary Figure 8 and 9.

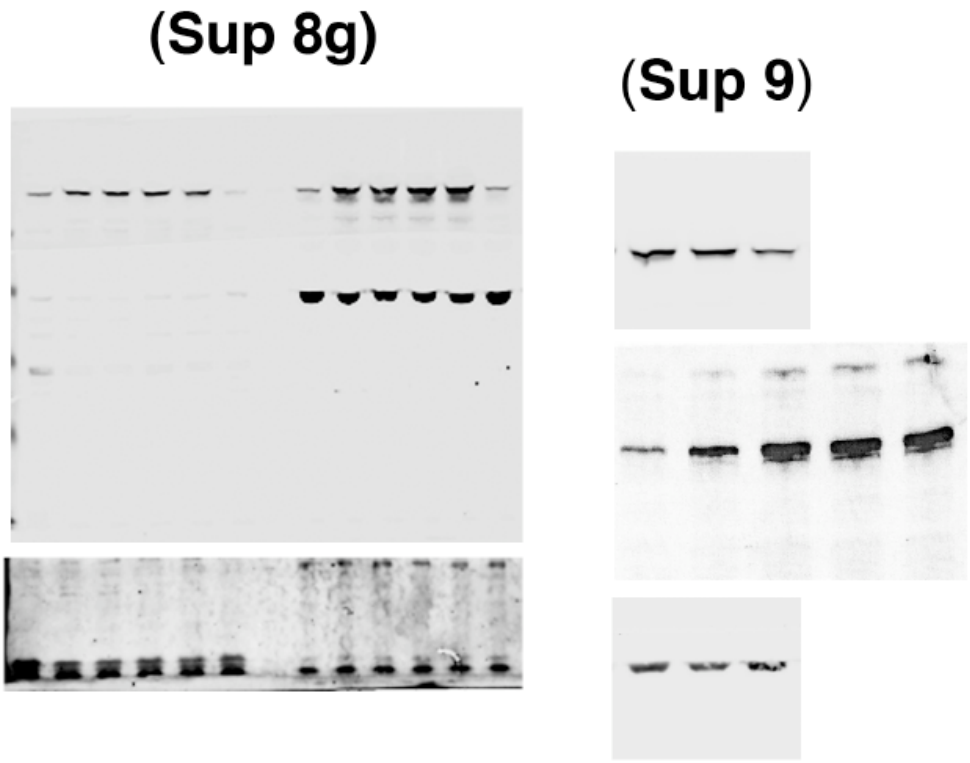

Supplementary Figure 24.

Full length gels for Supplementary Figure 10 and 11.

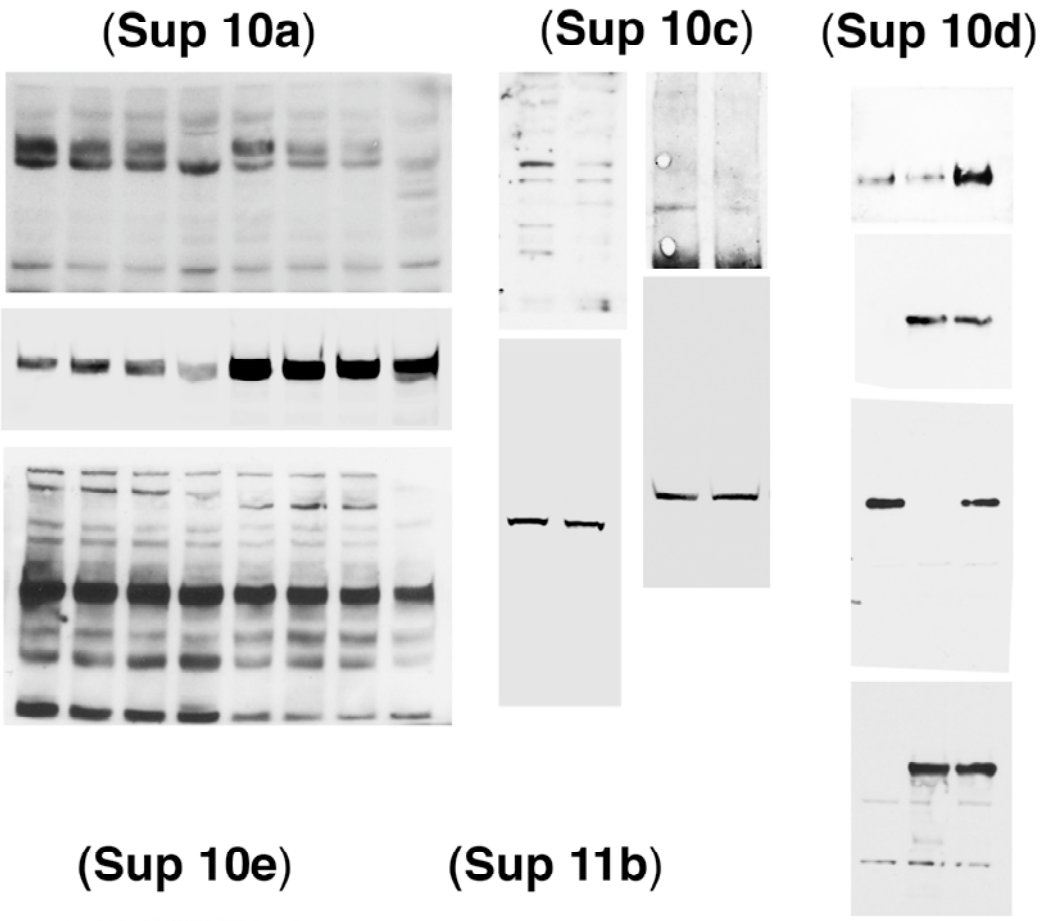

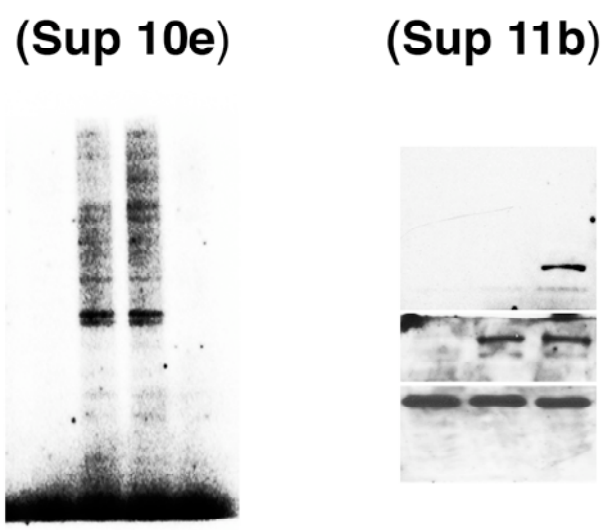

Table 1. Small molecule screening data

Category	Parameter	Description
Assay	Type of assay	*Xenopus* egg extract-based
	Target	The Wnt/β-catenin pathway (CTNNB1)
	Primary measurement	Detection of dual luciferase enzyme activities (Firefly luciferase and *Renilla* luciferase)
	Key reagents	Xenopus egg extract, β-catenin-FLuc and Axin-RLuc, LRP6ICD, Dual-Glo Luciferase Assay (Promega)
	Assay protocol	*Xenopus* egg extract preparation and degradation assays were performed as previously described[11]. β-catenin-FLuc and Axin-RLuc were generated in TNT SP6 High-Yield Protein Expression System (Promega). *In vitro*-translated (IVT) β-catenin-FLuc, Axin-RLuc, and LRP6ICD (400 nM) were added to 100 ml of egg extract and rotated end-over-end at 4°C for 10 minutes. Samples were dispensed into 384-well plates (5 μl/well) at 4°C prior to pin transfer of compounds at 25°C. Plates were sealed, vortexed, and incubated for 4 hours at 25°C. After incubation, firefly and *Renilla* luciferase activities were measured using the Dual-Glo Luciferase Assay on an EnVision plate reader (Perkin Elmer).
	Additional comments	A detailed description of the screen will be published elsewhere.
Library	Library size	2160
	Library composition	Known bioactive, NINDS custom collection, and Prestwick libraries
	Source	Institute for Chemistry and Cell Biology (ICCB), Harvard Medical School
	Additional information	http://iccb.med.harvard.edu/screening/compound_libraries/bioactives_ninds2.htm http://iccb.med.harvard.edu/screening/compound_libraries/Prestwick1_Collection.htm
Screen	Format	384-well, Corning 3705
	Concentration(s) tested	~40-200 μM, 2% DMSO
	Plate controls	Extract minus LRP6ICD
	Reagent/ compound dispensing system	Manual, using 24-channel repeat pipettor
	Detection instrument and software	EnVision (Perkin Elmer)
	Assay validation/QC	NINDS plates: Mean = 12.736387, Std. Deviation = 1.860133, Std. Error = 0.057405
	Normalization	According to Malo *et al.* (2006)[2]
Post-HTS analysis	Hit criteria	β-catenin FLuc/Axin RLuc ratio >3 standard deviations from the mean
	Hit rate	~1%
	Additional assay(s)	TOPflash Wnt signaling reporter assay in HEK 293 cells, *Xenopus* axis duplication assay, and immunoblotting for intra-cellular levels of β-catenin and Axin
	Confirmation of hit purity and structure	Compounds were repurchased (MP Biomedicals) and verified analytically

Supplementary Methods

Screen statistics

We normalized each plate using the method outlined in Malo et al.[2]. The normalization procedure uses Tukey's median polish[3] to remove systematic row and column biases (e.g. edge effects). Following normalization, a B-score value was obtained for each well that represents log intensities for each compound in a well. The differences of the log intensities between the Axin and β-catenin wells for each plate were obtained (equivalent to the ratio on the non-log scale). Compounds identified as hits (based on empirical distribution) in both replicates were added to the candidate list.

Antibodies

Immunoblotting was performed using the following antibodies: α-β-catenin (BD Transduction Labs); α-phospho-βcat (p33, 37, 41), α-MAPK 137F5, α-pSMAD1/5 41D10, α-SMAD1, α-pSTAT6 C11A12, α-STAT6 (Cell Signaling); mouse α-Axin1 (Zymed); goat α-Axin1 (R&D Antibodies); α-actin (ImmunO); α-ac-H3 (Upstate); α-Ki-67 (Abcam); α-ZO-1 (Invitrogen); α-HA 3F10 (Roche); rabbit α-hPygo2 H-216, rabbit α-CK1α (Santa Cruz); α-β-galactosidase, α-pMAPK (Promega); *Xenopus* β-catenin antibody (gift from Barry Gumbiner).

Plasmids

β-catenin-FLuc and Axin-RLuc fusions were generated using standard PCR-based cloning strategies and subcloned into the pCS2 vector. The bacterial expression construct of LRP6ICD has been described[4]. The following plasmids were gifts: HA-hPygo2 (Mariann Bienz), HA-TCF4 (Scott Hiebert), and HA-BCL9 (Konrad Basler).

Immunoblot analysis

Cells were lysed in non-denaturing buffer (50 mM Tris-Cl (pH 7.4), 300 mM NaCl, 5 mM EDTA, 1% (w/v) Triton X-100) and the soluble fraction used for immunoblotting.

For HA-tagged protein expression, cells were seeded in a 60-mm dish and transfected overnight (Lipofectamine 2000, Invitrogen) with 8 μg HA-tagged construct and 2 μg β-galactosidase (internal control). Cells were then split into separate wells, allowed to adhere, and treated as indicated. For cycloheximide (CHX)-chase experiments, cells were treated with 50 ug/ml CHX for the indicated time. For Axin immunoblots, Axin was immunoprecipitated with mouse anti-Axin antibodies (Zymed) and immunoblotted with anti-Axin1 goat antibody (R&D Antibodies). Cytoplasmic/nuclear fractionation was performed as follows. Cells were incubated on ice for 15 minutes in lysis buffer (10 mM HEPES (pH 7.8), 10 mM KCl, 2 mM $MgCl_2$, 0.1 mM EDTA), scraped, transferred to microfuge tubes, and NP-40 was added to 0.5%. Lysates were vortexed, sheared through a 23-gauge needle, and spun at 16,000Xg for 2 minutes. Supernatants (cytoplasmic fractions) were recovered. Pellets were resuspended in extraction buffer (50 mM HEPES (pH 7.8), 50 mM KCl, 300 mM NaCl, 0.1 mM EDTA, 10% glycerol), vortexed, incubated on ice for 30 minutes, centrifuged at 3,000Xg for 30 seconds, and supernatants discarded. Pellets were resuspended in extraction buffer, vortexed, spun at 3,000Xg and supernatants discarded. Pellets (nuclear fraction) were resuspended in RIPA buffer (50 mM Tris (pH 8.0), 150 mM NaCl, 1% NP40, 0.5% deoxycholic acid, 0.1% SDS, 0.5 mM EDTA).

Immunofluorescence

Cells were seeded on fibronectin-coated coverslips, fixed in 3.7% formaldehyde, stained, and mounted in VectaShield with DAPI (Vector Laboratories). Images were acquired using a CoolSNAP ES camera mounted on a Nikon Eclipse 80i fluorescence microscope with 60X or 100X objectives.

Real-time RT-PCR

Total RNA was isolated from HEK 293 cells 24 hours after pyrvinium treatment using RNAeasy RNA extraction kit (Qiagen) and cDNA generated using High Capacity

cDNA Reverse Transcription kit (Applied Biosystems, ABI). Real-time PCR assays were performed in quadruplicate using TaqMan Gene Expression Master Mix (ABI), gene-specific TaqMan TAMRA probes (ABI), and an ABI 7000 sequence detection system.

***Xenopus laevis* studies**

Xenopus embryos were *in vitro* fertilized, dejellied, maintained, and injected as previously described[5]. Pyrvinium was dissolved in 100% DMSO for injections. Capped *Xwnt8* mRNA was generated using mMessage mMachine (Ambion) according to manufacturer's instructions. Whole-mount *in situ* hybridization was performed as described for *chordin*[6,7]. Animal caps were excised from stage 9 embryos, cultured until stage 11, and RT-PCR for *siamois, Xnr3, XMif5, Xbra, and ODC* was performed as described[4,8].

***C. elegans* studies**

C*. elegans* were grown on a lawn of *E. coli* on plates containing nematode growth media (NGM). Pyrvinium was dissolved in either ethanol or DMSO. For vulval morphology experiments, worms were treated from L1 larval until adult stages (3 days) on plates containing pyrvinium (10 μM) or vehicle (1% ethanol). Worms were picked off plates and placed on glass slides for visual inspection of vulval morphology under Nomarski optics. Eggs retained in the uterus were counted for each treatment group and the two groups compared using a one-tailed t-test. Q neuroblast daughter cells, QL and QR, were marked by *mec-7*::GFP and Q neuroblast migration was scored in a fluorescence stereo dissecting scope by noting the location of touch neurons PVM (QL descendent) and AVM (QR descendent) at the L4 larval stage.[9] The nematode strain *KN562* [*pop-1(hu9); muIs32 (mec-7::*GFP + *lin-15(+)*) was used to evaluate Q cell migration in a *pop-1* mutant background. For all of these experiments, the observer was blinded to the specific treatment to avoid bias.

Limited trypsin digest

Recombinant CK1α or GSK3 (0.5 ug each) were preincubated for 5 min at RT in the absence or presence of pyrvinium (100 nM) followed by incubation at RT with bovine pancreatic trypsin (50 ng). After 10 minutes, excess soybean trypsin inhibitor was added and samples analyzed by SDS-PAGE followed by silver staining.

Supplementary Chemical Compound Information

(Performed by the Vanderbilt Chemical Synthesis Core)

General: All NMR spectra were recorded on a Varian Inova 400 (400 MHz) spectrophotometer located in the Small Molecule NMR Facility at Vanderbilt University. 1H chemical shifts are reported in δ values in ppm downfield from TMS as the internal standard. Data are reported as follows: chemical shift, multiplicity, coupling constant (Hz), integration. Splitting patterns describe apparent multiplicities and are designated as s (singlet), d (doublet), t (triplet), q (quartet), m (multiplet), br (broad). 13C chemical shifts are reported in δ values in ppm. Low-resolution mass spectra were obtained on an Agilent 1200 LCMS with electrospray ionization. High-resolution mass spectra were recorded on a Waters Qtof- API-US plus Acquity system. Analytical thin layer chromatography was performed on 250 mM silica gel 60 F254 plates. Analytical HPLC was performed on an Agilent 1200 analytical LCMS with UV detection at 214 nm and 254 nm along with ELSD detection. Flash column chromatography was performed on silica gel (230-400 mesh, Merck) or using automated silica gel chromatography (Isco, Inc. 100sg Combiflash).

Preparation of IWR-1

IWR-1 was prepared according to published methods, with all characterization data in agreement.[10]

Preparation of VU-WS211

1-(2,5-Dimethyl-1-phenyl-1*H*-pyrrol-3-yl)-2-(quinolin-2-yl)ethanol: A solution of 2-methylquinoline (0.27 mL, 2.0 mmol) in THF (7 mL) was cooled to -78 ^{o}C. To this solution was added *n*-BuLi in hexanes (2.5 M, 0.88 mL, 2.21 mmol), and the mixture was allowed to warm 0 ^{o}C and stirred for 60 min followed by warming to room temperature with additional stirring for 30 min. The reaction was cooled (-78 ^{o}C) and 2,5-dimethyl-1-phenyl-1H-pyrrole-3-carbaldehyde (0.4 g, 2.0 mmol) in THF (2 mL) was added over 5 min. The reaction mixture was allowed to warm to room temperature over a 60 min period, stirred for 3 h, diluted in ethyl acetate, and then washed with saturated NH_4Cl (3 x 10 mL). The organic phase was dried over $MgSO_4$ and evaporated *in vacuo* affording crude product which was purified by flash column chromatography on silica gel (hexane/ethyl acetate = 4/1) to provide oil product **1** (0.59 g, 86%). ^{1}H NMR ($CDCl_3$, 400 MHz) ∂ (ppm) 8.09 (dd, *J* = 4.0, 8.4 Hz, 2H), 7.80 (d, *J* = 8.0 Hz, 1H), 7.71 (t, *J* = 7.2 Hz, 1H), 7.52 (t, *J* = 7.2 Hz, 1H), 7.46 (t, *J* = 7.2 Hz, 2H), 7.39 (t, *J* = 7.2 Hz, 1H), 7.30 (d, *J* = 8.4 Hz, 1H), 7.22 (d, *J* = 7.6 Hz, 2H), 6.13 (s, 1H), 5.34 (dd, *J* = 2.4, 10.0 Hz, 1H), 3.58 (dd, *J* = 10.0, 15.6 Hz, 1H), 3.31 (dd, *J* = 2.4, 15.6 Hz, 1H), 2.05 (s, 6H); ^{13}C NMR ($CDCl_3$, 100 MHz) ∂ (ppm) 161.34, 147.20, 138.83, 136.42, 129.53, 128.96, 128.78, 128.35, 128.27, 127.57, 127.48, 126.77, 125.95, 125.42, 122.20, 121.43, 104.19, 66.63, 45.44, 12.87, 10.85; LCMS showed dehydrated peak.

(*E*)-2-(2-(2,5-Dimethyl-1-phenyl-1*H*-pyrrol-3-yl)vinyl)quinoline (VU-WS211): To a solution of 1-(2,5-dimethyl-1-phenyl-1H-pyrrol-3-yl)-2-(quinolin-2-yl)ethanol (0.59 g, 1.82 mmol) in dichlromethane (9 mL) were added MsCl (0.28 mL, 3.64 mmol) and pyridine (0.44 mL, 5.46 mmol) at 0 ^{o}C. The reaction mixture was allowed to warm to room temperature, stirred overnight, and then washed with saturated NH_4Cl (3 x 10 mL). The resulting aqueous solution was extracted with CH_2Cl_2 (3 x 15 mL). The combined organic layer was dried over $MgSO_4$ and evaporated. The crude product was purified by

flash column chromatography on silica gel (hexane/ethyl acetate = 4/1) to provide **VUWS211** (0.24 g, 41%). ^{1}H NMR ($CDCl_3$, 400 MHz) d (ppm) 8.04 (t, *J* = 8.0 Hz, 2H), 7.74-7.61 (m, 4H), 7.48 (t, *J* = 7.6 Hz, 2H), 7.42 (t, *J* = 7.6 Hz, 2H), 7.22 (d, *J* = 7.6 Hz, 2H), 7.06 (d, *J* = 16.0 Hz, 1H), 6.38 (s, 1H), 2.19 (s, 3H), 2.05 (s, 3H); ^{13}C NMR ($CDCl_3$, 100 MHz) d (ppm) 157.47, 148.27, 138.23, 135.77, 130.34, 130.26, 129.35, 129.16, 128.70, 128.13, 128.01, 127.70, 127.33, 126.80, 125.17, 123.37, 118.84, 118.20, 103.53, 12.83, 10.96; LCMS, single peak, 1.36 min, *m/e*, 325.2 (M+1); m.p.: 58 - 60^{o}C; HRMS (ESI TOF) calcd for $C_{23}H_{21}N_2$ $(M + H)^+$ 325.1705, found 325.1703.

Preparation of pyrvinium iodide

(*E*)-2-(2-(2,5-Dimethyl-1-phenyl-1*H*-pyrrol-3-yl)vinyl)-*N*,*N*-dimethylquinolin-6-amine: This compound was synthesized by the same methods used above, except using N,N,2-trimethylquinolin-6-amine. ^{1}H NMR ($CDCl_3$, 400 MHz) *∂* (ppm) 7.91 (d, *J* = 9.6 Hz, 1H), 7.87 (d, *J* = 8.8 Hz, 1H), 7.57-7.38 (m, 5H), 7.32 (dd, *J* = 2.8, 9.2 Hz, 1H), 7.21 (d, *J* = 6.8 Hz, 2H), 7.02 (d, *J* = 16.0 Hz, 1H), 6.78 (d, *J* = 2.4 Hz, 1H), 6.35 (s, 1H), 3.06 (s, 6H), 2.16 (s, 3H), 2.04 (s, 3H); ^{13}C NMR ($CDCl_3$, 100 MHz) *∂* (ppm) 153.62, 148.02, 138.40, 134.23, 130.10, 129.65, 129.16, 128.22, 127.95, 125.66, 123.69, 119.27, 118.93, 118.40, 105.52, 103.51, 40.77, 12.88, 10.98; LCMS, single peak, 1.48 min, *m/e*, 368.2 (M+1); m.p.: 158 – 161^{o}C; HRMS (ESI TOF) calcd for $C_{25}H_{26}N_3$ $(M + H)^+$ 368.2127, found 368.2123.

Pyrvinium iodide ((*E*)-2-(2-(2,5-dimethyl-1-phenyl-1*H*-pyrrol-3-yl)vinyl)-6-(dimethylamino)-1-methylquinolin-1-ium iodide): A mixture of (E)-2-(2-(2,5-dimethyl-1-phenyl-1H-pyrrol-3-yl)vinyl)-N,N-dimethyl quinolin-6-amine (100 mg, 0.27 mmol), methyl iodide (20 mL, 0.33 mmol), and toluene (3 mL) was heated in a sealed tube at 80 ^{o}C for 24 h. The solvent was removed *in vacuo* and then triturated with ethyl acetate (3 x 7 mL) to provide a red solid product (90 mg, 87 %). ^{1}H NMR (DMSO, 400 MHz) *∂* (ppm); 8.51 (d, *J* = 9.2 Hz, 1H), 8.44 (d, *J* = 9.2 Hz, 1H), 8.21 (d, *J* = 10.0 Hz, 1H), 8.08 (d, *J* =

15.2 Hz, 1H), 7.61 – 7.49 (m, 4H), 7.35 (d, *J* = 7.6 Hz, 2H), 7.23 (d, *J* = 8.0 Hz, 1H), 7.21 (d, *J* = 10.0 Hz, 1H), 6.72 (s, 1H), 4.35 (s, 3H), 3.10 (s, 6H), 2.23 (s, 3H), 2.00 (s, 3H); ^{13}C NMR ($CDCl_3$, 100 MHz) ∂ (ppm) 151.55, 148.81, 139.84, 138.92, 136.93, 135.96, 131.37, 131.29, 129.61, 128.74, 128.69, 127.93, 127.85, 121.39, 120.09, 119.51, 119.04, 111.64, 106.40, 104.65, 40.34, 38.45, 12.65, 10.82; LCMS, single peak, 1.55 min, *m/e*, 383.7 (M+1); m.p.; 255 – 258 ^{o}C; HRMS (ESI TOF) calcd for $C_{26}H_{28}N_3$ $(M + H)^+$ 382.2283, found 382.2282.

Preparation of VU-WS113

***N*-(6-bromoquinolin-2-yl)-2,5-dimethyl-1-phenyl-1H-pyrrole-3-carboxamide:**

In a conical shaped microwave vial was added 2-amino-6-bromoquinoline hydrochloride (100 mg, 0.385 mmol) and dichloroethane (DCE, 3.8 mL). To this suspension was added Hunig's base (0.30 mL, 1.73 mmol). The solution turned deep brown and the solids dissolved. 2,5-dimethyl-1-phenyl-1H-pyrrole-3-carboxylic acid (107 mg, 0.501 mmol) and 1-[chloro(pyrrolidin-1-yl)methylene]pyrrolidin-1-ium hexafluorophosphate(V) (PyClU, 256 mg, 0.771 mmol) were added. The microwave vial was capped and heated under microwave irradiation for 1.5 h at 110 °C. After cooling, the solution was concentrated and the residue was purified on silica gel using a Biotage SNAP cartridge (2% to 20% MeOH in dicholormethane) to yield 144 mg (0.34 mmol, 89%) of the desired compound as a beige powder. LCMS: R_T = 1.44 min, >90% @ 254 nm, >92% @ 220 nm; *m/z* $(M + 1)^+$ = 420. ^1H NMR (400 MHz, CD_3OD, δ (ppm)): 8.6 (d; *J* = 9.2 Hz; 1 H), 8.0 (d; *J* = 9.2 Hz; 1H), 7.9 (s; 1H), 7.8 (s; 1H), 7.5-7.4 (m; 4H), 7.2 (d; J = 6.8 Hz; 2H), 6.3 (s; 1H), 2.4 (s; 3H), 2.0 (s; 3H). ^{13}C NMR (100 MHz; CD_3OD, δ (ppm)): 164.4, 152.4, 145.5, 137.6, 137.3, 136.5, 133.2, 129.7, 129.6, 129.4, 129.0, 128.9, 128.2, 127.3, 118.1, 115.6, 133.8, 104.9, 12.9, 12.7. HRMS calculated for $C_{22}H_{19}N_3OBr$ $(M+H)^+$ *m/z*: 420.0711, measured 420.0707.

2,5-dimethyl-N-(6-(morpholinomethyl)quinolin-2-yl)-1-phenyl-1H-pyrrole-3-carboxamide (VU-WS113): In a conical shaped microwave vial was added N-(6-bromoquinolin-2-yl)-2,5-dimethyl-1-phenyl-1H-pyrrole-3-carboxamide (71 mg, 0.169 mmol), potassium trifluoro(morpholinomethyl)borate (70 mg, 0.338 mmol), 2-Dicyclohexylphosphino-2′,4′,6′-triisopropylbiphenyl (XPhos, 16.1 mg, 0.034 mmol), cesium carbonate (165 mg, 0.507 mmol), and palladium (II) acetate (3.8 mg, 0.017 mmol), THF (0.63 mL) and water (0.06 mL). The microwave vial was capped and the solids were stirred at RT for 5 min to aid in dissolution. Once a clear solution was observed, the vial was heated to 80 °C for 10 min followed by heating to 145 °C for 45 min. After cooling, the solution was diluted with dichloromethane and dried over $MgSO_4$. The solution was filtered, concentrated and purified on silica gel using a Biotage SNAP cartridge (2 % to 20% MeOH in dichloromethane) to yield 71 mg (0.16 mmol, 95%) of VU-WS113 as a yellow oil: LCMS: R_T = 1.11 min; *m/z* $(M + 1)^+$ = 441. ^1H NMR (400 MHz, $CDCl_3$, δ (ppm)): 8.4 (d; *J* = 8.8 Hz; 1H), 8.3 (d; *J* = 8.8 Hz; 1H), 7.8-7.7 (m; 5H), 7.3 (d; *J* = 7.2Hz; 2H), 6.5 (s; 1H), 3.8-3.7 (m; 10H), 2.5-2.4 (m; 8H), 2.3 (s; 3H), 2.0 (s; 3H). ^{13}C NMR (100 MHz; $CDCl_3$, δ (ppm)): 166.7, 152.0, 147.3, 139.5, 138.9, 135.6, 132.8, 130.7, 130.5, 130.0, 129.5, 129.4, 129.1, 128.0, 127.1, 116.2, 114.9, 106.3, 67.8, 64.0, 54.7, 12.8, 12.7. HRMS calculated for $C_{27}H_{29}N_4O_2$ $(M+H)^+$ *m/z*: 441.2291, measured 441.2291.

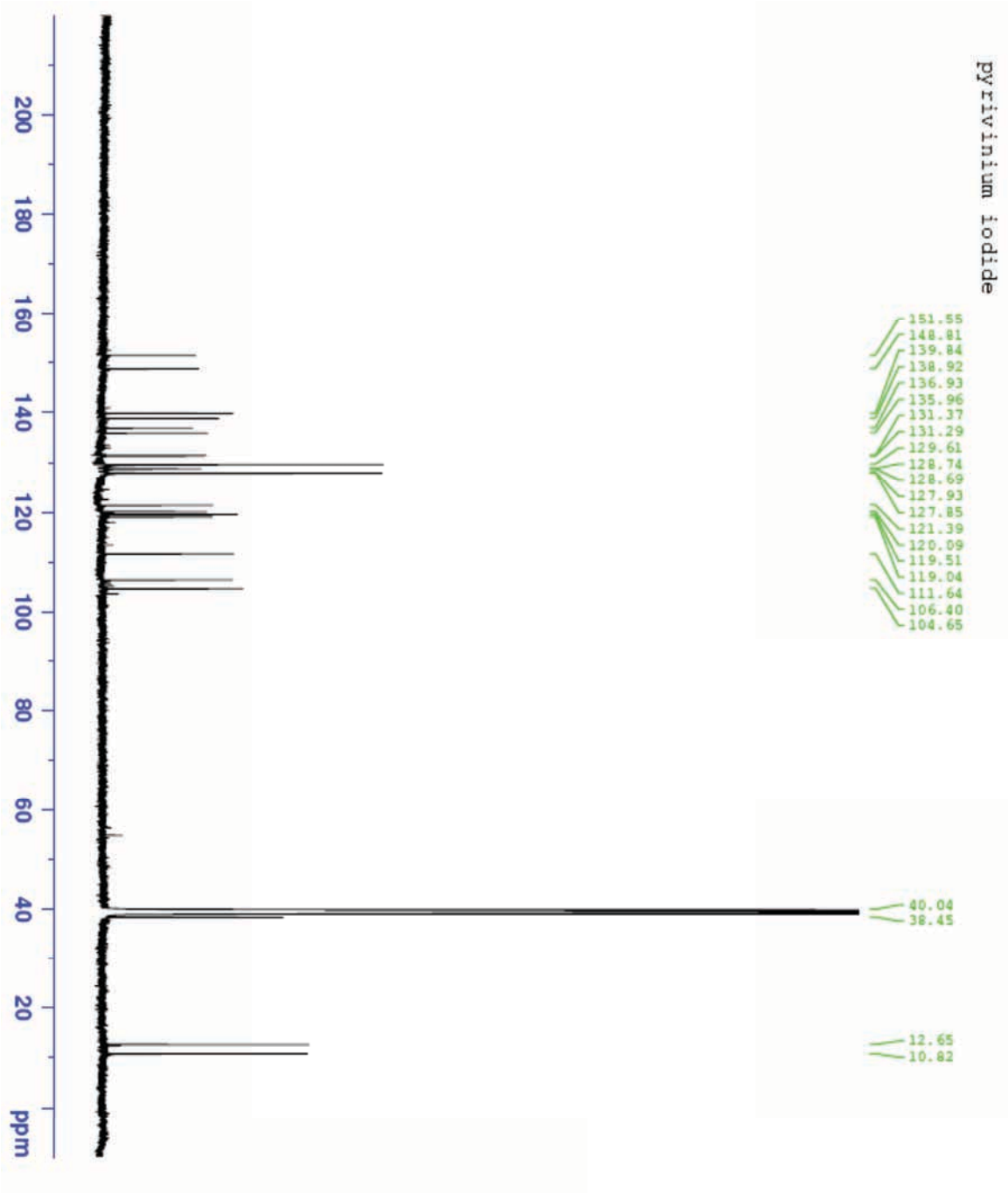

Nature Chemical Biology: doi: 10.1038/nchembio.453

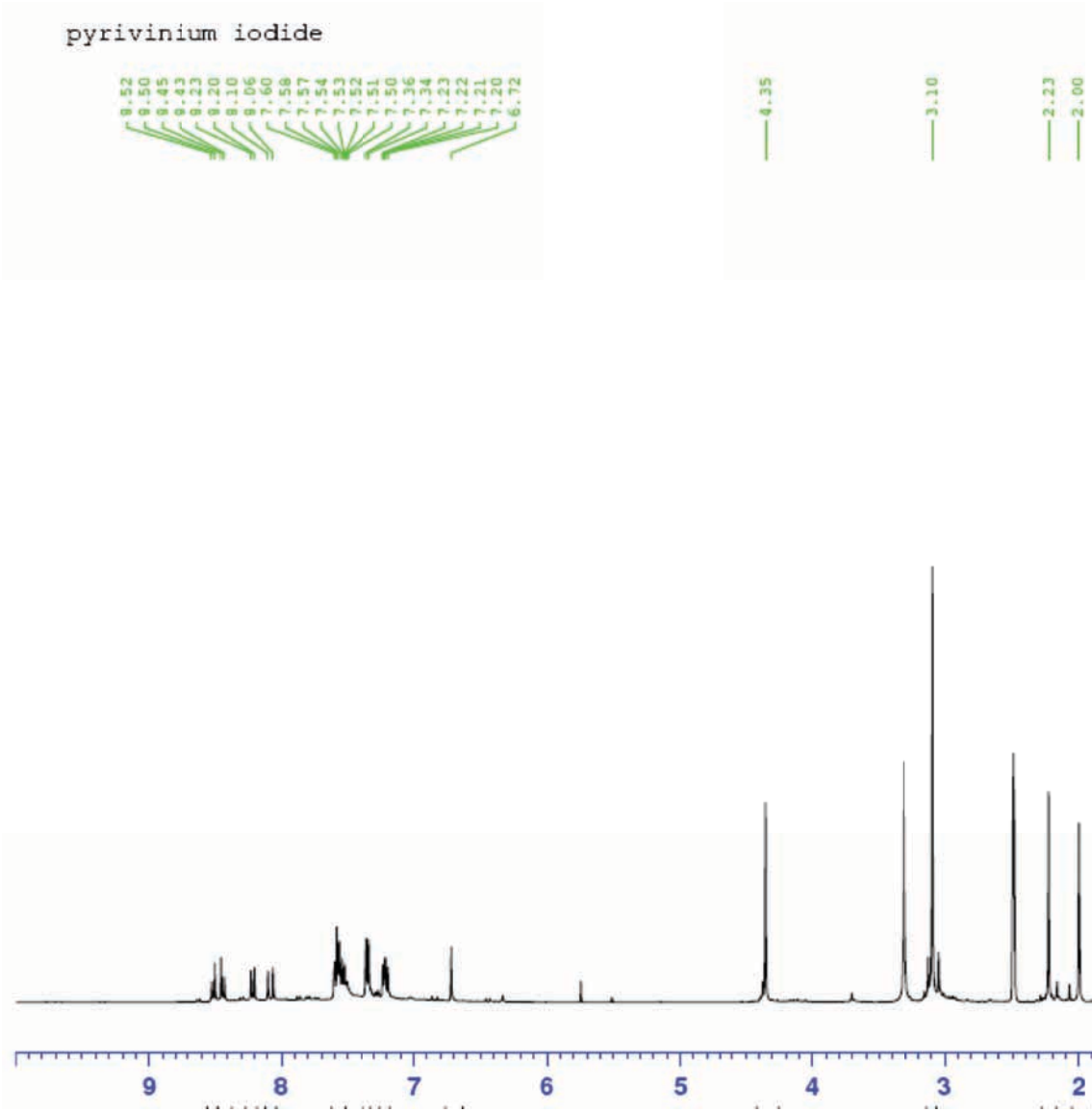

Nature Chemical Biology: doi: 10.1038/nchembio.453

VU-WS113

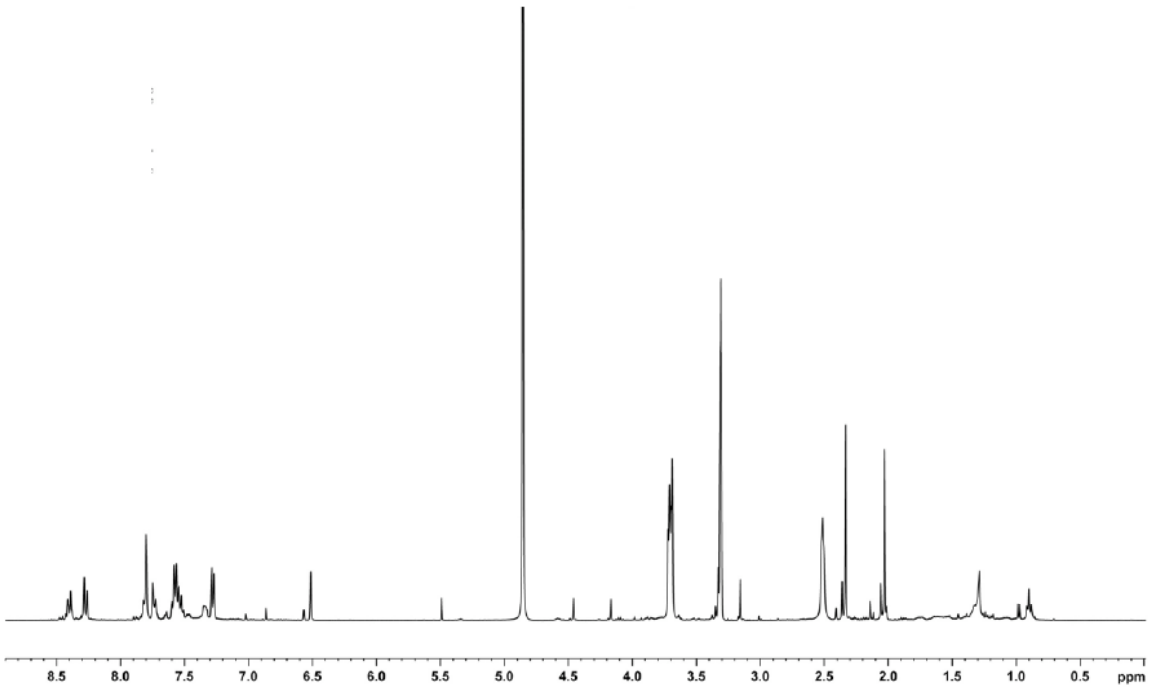

VU-WS113

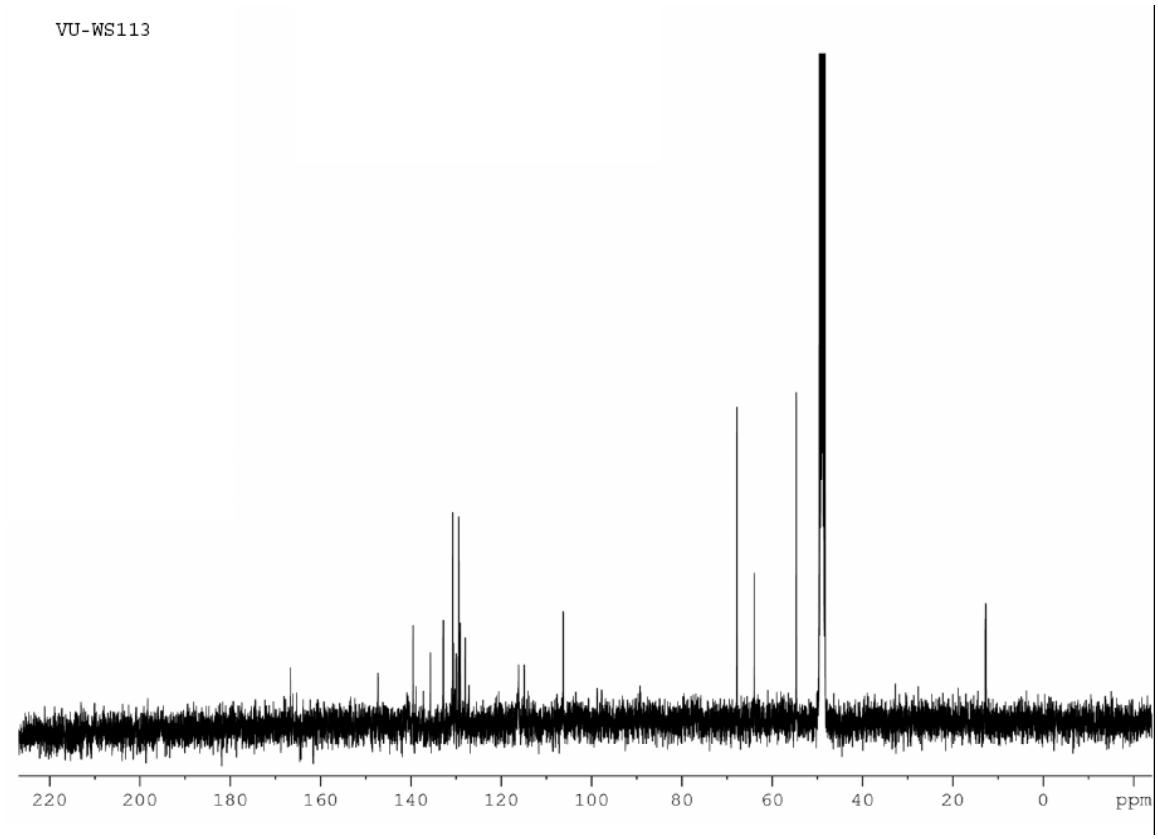

Nature Chemical Biology: doi: 10.1038/nchembio.453

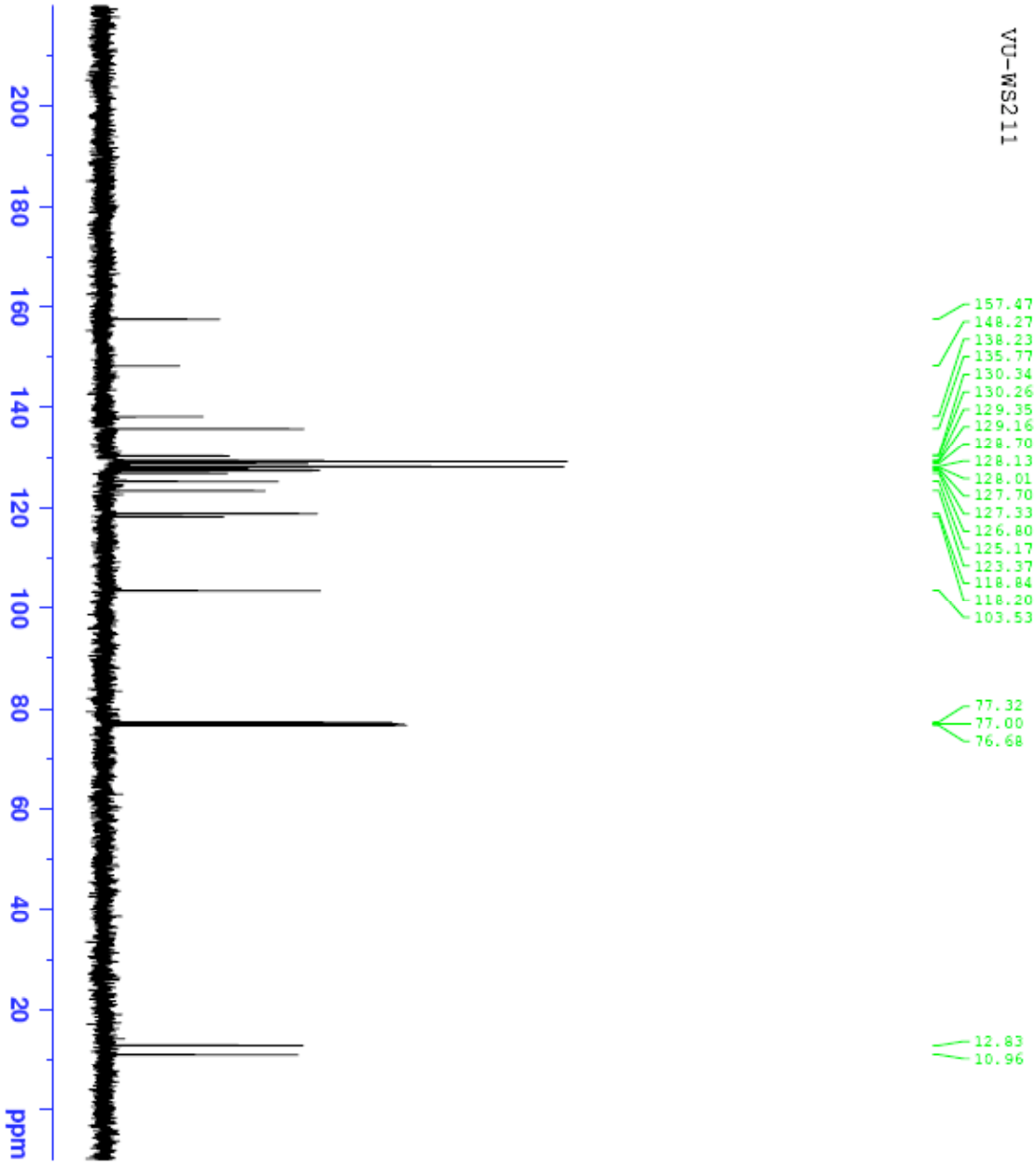

Nature Chemical Biology: doi: 10.1038/nchembio.453

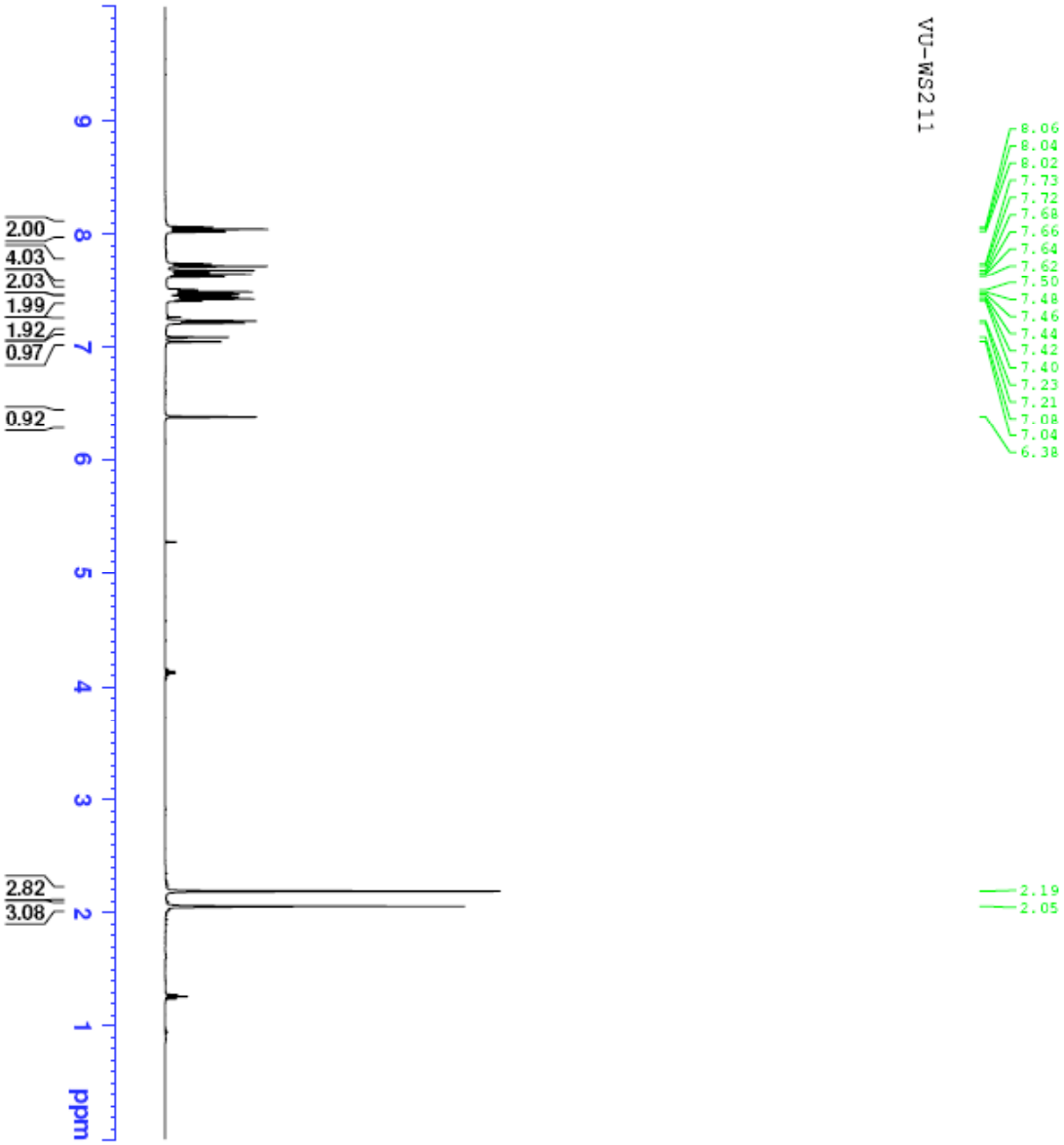

Nature Chemical Biology: doi: 10.1038/nchembio.453

Supplementary References

1. Huppert, S.S., Ilagan, M.X., De Strooper, B., & Kopan, R., Analysis of Notch function in presomitic mesoderm suggests a gamma-secretase-independent role for presenilins in somite differentiation. *Dev Cell* 8 (5), 677-688 (2005).
2. Malo, N., Hanley, J.A., Cerquozzi, S., Pelletier, J., & Nadon, R., Statistical practice in high-throughput screening data analysis. *Nat Biotechnol* 24 (2), 167-175 (2006).
3. Tukey, J.W., Exploratory data analysis (Reading, Mass.: Addison-Wesley Pub. Co.). (1977).
4. Cselenyi, C.S. *et al.*, LRP6 transduces a canonical Wnt signal independently of Axin degradation by inhibiting GSK3's phosphorylation of beta-catenin. *Proc Natl Acad Sci U S A* 105 (23), 8032-8037 (2008).
5. Peng, H.B., Xenopus laevis: Practical uses in cell and molecular biology. Solutions and protocols. *Methods Cell Biol* 36, 657-662 (1991).
6. Harland, R.M., In situ hybridization: an improved whole-mount method for Xenopus embryos. *Methods Cell Biol* 36, 685-695 (1991).
7. Sasai, Y. *et al.*, Xenopus chordin: a novel dorsalizing factor activated by organizer-specific homeobox genes. *Cell* 79 (5), 779-790 (1994).
8. Lemaire, P. & Gurdon, J.B., A role for cytoplasmic determinants in mesoderm patterning: cell-autonomous activation of the goosecoid and Xwnt-8 genes along the dorsoventral axis of early Xenopus embryos. *Development* 120 (5), 1191-1199 (1994).
9. Ch'ng, Q. *et al.*, Identification of genes that regulate a left-right asymmetric neuronal migration in Caenorhabditis elegans. *Genetics* 164 (4), 1355-1367 (2003).
10. Chen, B. *et al.*, Small molecule-mediated disruption of Wnt-dependent signaling in tissue regeneration and cancer. *Nat Chem Biol* 5 (2), 100-107 (2009).
11. Murray, A.W., Cell cycle extracts. *Methods Cell Biol* 36, 581-605 (1991).